International Journal of Scientific Research Updates

Journal homepage: https://orionjournals.com/ijsru/

ISSN: 2783-0160 (Online)

(RESEARCH ARTICLE)

Trypanosoma cruzi kDNA minicircle sequences integration into the vertebrate host genome: A biomarker for monitoring the efficacy of multidrug treatment of Chagas disease

Antonio Raimundo Lima Teixeira [1, *] Clever Cardoso Gomes [2], Adriana Alves Sá [1, 3], Rubens José Nascimento [1], [4], Liana Lauria-Pires [1, 5], Ana Maria Castro [6], Francisco Ernesto Moreno Bernal [7] and Alessandro Oliveira de Sousa [1, 8]

[1] *Department of Pathology, Faculty of Medicine of the University of Brasília. CEP 70.910-900, Federal District, Brazil.*
[2] *Department of Histology, Embryology and Cell Biology, Federal University of Goiás. CEP 74605-90, Goiânia Brazil.*
[3] *Sambaia Regional Hospital, QS 614, Cj C, Block* 1/2, South Samambaia. CEP 72322-583, Federal District, Brazil.
[4] *National Technical Commission on Biosafety, Ministry of Science and Technology. South Police Sector, Area 5, Block 3, Block B, Rooms 10 to 14. CEP 70610-200, Brasília, Federal District, Brazil.*
[5] *Catholic University of Brasilia, Department of Medicine, Taguatinga. CEP 71966-700, Federal District, Brazil.*
[6] *Institute for Tropical Pathology and Public Health, Federal University of Goiás. CEP 74605-050, Goiânia, Brazil.*
[7] *Animal Welfare and Avian Pathology Laboratory, Faculty of Agronomy and Veterinary Medicine, University of Brasília, CEP 70910-900, Federal District, Brazil.*
[8] *Logistic Office for Health, Federal District Health Department, Building PO700, 2nd* Floor, SRTV 702, W5 North. CEP 70723-040, Brasília, Brazil.

International Journal of Scientific Research Updates, 2023, 05(01), 170–207

Publication history: Received on 01 February 2023; revised on 10 March 2023; accepted on 13 March 2023

Article DOI: https://doi.org/10.53430/ijsru.2023.5.1.0026

Abstract

The protist *Trypanosoma cruzi* inserts kinetoplast DNA minicircle sequences into the host genome. Sensitive PCR with specific primer sets revealed protozoan nuclear DNA and kinetoplast DNA in agarose gels bands probed with radiolabel specific sequences for tissues of *T. cruzi*-infected rabbits and mice. Avian species are refractory to the infection, but chicks that hatched from *T. cruzi*-inoculated eggs retained the kinetoplast DNA in the embryonic germ line cells and developed parasite-free Chagas disease-like cardiomyopathy. A Target-primer TAIL-PCR with specific primer sets, Southern hybridization, cloning, and sequencing of the amplification products revealed kinetoplast minicircle sequences integration sites mainly in LINE-1 transposable elements and hitchhiking to several loci. This kinetoplast DNA biomarker was used to monitor the effect of multidrug treatment of *T. cruzi*-infected mice. A trypanocidal nitro heterocyclic compound in combination with an array of inhibitors of eukaryotic cell division prevented minicircle sequences transfer. Nine out of 12 inhibitors prevented the kinetoplast DNA integration into the macrophage genome. The multidrug treatment of *T. cruzi*-infected mice with benznidazole, azidothymidine and ofloxacin lowered the rate of minicircle sequences integrations into the mouse genome by 2.44-fold and reduced the rejection of the target heart cells.

Keywords: *Trypanosoma cruzi*; kDNA transfer; Biomarker; Multidrug treatment; Chagas disease

1 Introduction

The *Trypanosoma cruzi* agent of Chagas disease is a Protist flagellate showing a symbiotic mitochondrion with circa a dozen maxicircles and twenty thousand catenated minicircles [1, 2]. The thousand copies of minicircles average 1.4 kb in size, each with four conserved 238 base pairs (bp) regions interspersed by four variable sequences of 122 bp intercalated sequence blocks CSB1, CSB2, and CSB3 [3]. *T. cruzi* population from different ecosystems have been partitioned into TcI to TcIV discrete type units (DTUs). The comparative genome analyses from various DTUs displayed genetic variability correlation with natural and experimental infection. [4-6].

* Corresponding author: Antonio Raimundo Lima Teixeira

Copyright © 2023 Author(s) retain the copyright of this article. This article is published under the terms of the Creative Commons Attribution Liscense 4.0.

The American trypanosomiasis infections span an extensive geographical area in the American Continents, were autochthonous, zoonotic *T. cruzi* infection spreads among mammal's species. The human migration spread the Chagas disease to five Continents [7-10].

Early-phase *T. cruzi* infections in humans are usually not perceived by an individual with flagellates in their blood [11]. Life-long infections can occur in the absence of overt symptoms and signs. However, approximately one-third of chronically *T. cruzi*-infected humans develop clinical disease, averaging 45 ± 10 years after onset of infection [12]. The diagnosis is confirmed by serologic and nucleic acid assays [13, 14]. The disease affects the heart (94.5%) and the digestive system (mega esophagus and megacolon syndromes, 5.5%) [15, 16]. The family-based Chagas disease is a prevalent cause of heart failure in the Western Hemisphere [17]. The lead heterocyclic benzylimidazole [N-Benzyl-2-(2-nitro-1H-imidazol-1-yl) acetamide] has been used for the treatment of *T. cruzi* infections [18-20]. The nitro heterocyclic toxicity to eukaryotic cells stems from reductase enzyme nitro anion radicals (R-(NO^{2-}) and free O^{2-}, OH^{-} and H^2O^{2-} [21, 22].

Understanding the pathogenesis of the disease is essential to achieve drug treatment objectives [23-30]. In this regard, the rodent (*Mus musculus*) model, which is amenable to *T. cruzi* infections are mostly used to monitor the treatment of the disease [18, 20, 30]. Rabbits (*Oryctolagus cuniculus*) are relatively resistant to early infection, but they die of chronic Chagas heart disease [31-34].

In this study, the pathogenesis of the hallmark Chagas-like cardiomyopathy was investigated in a chicken model system refractory to *T. cruzi* infections [23, 35, 36]. The chicks that hatched from *T. cruzi*-infected eggs integrated the kDNA minicircle sequences in their genomes and died of chronic Chagas-like heart disease. Herein, we advance the hypothesis the kDNA integration in the hosts' genome is a biomarker of pathology and, therefore, the Chagas heart disease requires multidrug treatment with a trypanocide drug mixed with inhibitors of eukaryotic cell metabolic pathways of cell growth and differentiation. In this respect, some features of metabolic pathways of eukaryote cell growth and differentiation checkpoints are briefly reviewed.

Protein kinase-dependent cyclins (Cdk) phosphorylate serine-threonine protein inducers of the cell growth (G1), synthesis (S), (G2) and mitosis (M) cycle [37, 38]. A class of cyclins binds the Cdk at the S1 phase and are required for inception of the cell cycle S phase, and other class required to induce cell growth. The expression of the cyclins activates CDK4, and CDK6 phosphorylates proteins that promotes transition from cell growth (G1) to synthesis (S) phase (39, 40]. Mitogen-activated protein kinases (MAPK) play a role in the regulation of cyclin-dependent, serine-threonine protein kinases (MAPKs), glycogen synthase kinase-3 (GSK3) and CDK-like (CDKL) kinases in eukaryotic cells and are involved in the cascade of cell growth and differentiation. The phosphorylation activated serine-threonine kinases (MAPKK) include 14 family members identified in mammalian cells [41]. In addition, extracellular signal-regulated kinases (ERK1 and 2), c-Jun N-terminal kinase (JNK), and their additional isoforms carry out protein phosphorylation [42]. PI3K receptors with protein kinase activity and G protein receptors are inducers of autophosphorylation. In addition, the serine-threonine protein kinase C (PKC) isoforms activated by Ca++ released from the endoplasmic reticulum by diacylglycerol (DAG) and inositol 1,4,5-triphosphate (IP3), contribute to cell growth pathways [42].

The hypothesis to prevent the Chagas disease pathological manifestations is set forward, which consisted of multidrug treatment with a lead nitro heterocyclic to inhibit the parasitic load, and the integration of kDNA minicircle sequence with inhibitors of metabolic pathways of eukaryotic cell growth. The investigations revealed *Trypanosoma cruzi* kDNA minicircle sequences integrations in transposable elements of the host's genome. The treatment of *T. cruzi*-infected mice with benznidazole, azidothymidine, and ofloxacin lowered the ratio of kDNA mutations. Consequently, the *T. cruzi*-infected and treated mice displayed no or minimal rejection of heart cells by immune lymphocytes.

2 Methods

2.1 Collection of Human Blood

Chagas disease patients volunteered to participate in this study and donated 10 ml of blood. Serum samples were collected and subjected to immunological testing for *T. cruzi* antibodies, and the blood-nucleated cells yielded DNA for biotechnological analyses.

2.2 Growth of Eukaryotic Cells

The Berenice *T. cruzi* was grown in 5 ml of liver-infusion-tryptose (LIT) medium in screw-cap glass tubes kept on a shaker-incubator at 27 ºC, and a clone of the Tulahuén *T. cruzi* stock expressing β-galactose [43] was grown in complete

Dulbecco Minimum Essential Medium (cDMEM) [44]. The *T. cruzi* epimastigotes grown in axenic LIT medium were employed to determine the optimal doses of drug inhibitors of cell growth and development. The *Leishmania brasiliensis* LTB300 stock promastigote forms harvested in the exponential growth phase were collected from the culture medium; the cells were washed three times in PBS, pH 7.4, were collected by centrifugation, and were used in the experiments. The materials, equipment's, and laboratory animals used in these experiments are shown in supplementary information S1 Table.

The L6 murine muscle cells and the human macrophage cell line U937 were maintained by serial passaging in sterile culture flasks containing freshly prepared cDMEM. The cell line grown in 15 mL culture flasks was inoculated with 10 x 10^4 trypomastigotes. After several cycles of divisions, the host cell-loaded amastigotes differentiated into trypomastigotes that emerged in the supernatant. The flagellates were collected by centrifugation at 3,000 x g for 15 min in a swing bucket rotor, were washed three times and resuspended in FBS-free DMEM. [44]. The trypomastigotes were used in *ex vivo* drug inhibitor experiments and to infect the experimental animals to model Chagas disease.

To investigate the macrophages-*T. cruzi* interactions, aliquots of 10 x 10^4 uninfected macrophages grown in cDMEM, pH 7.2, were incubated at 37 ºC, forming monolayers in the culture flasks inoculated with 5 x 10^4 *T. cruzi* trypomastigotes in 5 mL of DMEM. At day 14 post-infection the macrophages were released with 0.25 M trypsin, washed three times with PBS, pH 7.2, and subjected to DNA extraction.

2.3 Assessment of the Cytotoxic Effect of Drug Inhibitors on *T. cruzi*-Infected Muscle Cells

The L6 muscle cell monolayers grown in glass chamber were inoculated with 10 x 10^3 trypomastigotes suspended in 3 mL cDMEM. One week after *T. cruzi* inoculation, the muscle cells loaded with the dividing amastigotes were treated with a concentration of a specific eukaryotic cell growth inhibitor. The optimal drug concentration was determined in triplicate dose-response assays, which showed absent, discrete, moderate, or severe toxic effects on the *T.* cruzi-infected host cells during two weeks in a CO_2 incubator at 37 ºC. The concentration of the drug inhibitor that did not kill muscle cells were identified under an inverted microscope.

2.4 Hosts Cells' DNA Extraction

T. cruzi-infected macrophage monolayers were collected by centrifugation and washed once with PBS, pH 7.4. After two washes with TBS (20 mM Tris-HCl pH 7.2, 0.5M NaCl) the cell pellets were obtained by centrifugation at 1,500 x g for 15 min and resuspended in 2 mL of extraction buffer (1 mM Tris-HCL, pH 8.0, 0.1 M EDTA, 0.5% SDS, 200 ng/mL RNase). Thereafter, proteinase K (100 µg/mL) was added, and the incubation period was extended for 12 h. The cells in the pellet were subjected to two extractions with an equal volume of chlorophenol (phenol: chloroform: isoamyl, 25:24:1) and a further extraction with chlorophyl (chloroform: isoamyl alcohol, 24:1) under light agitation at room temperature. The aqueous and organic phases were separated by centrifugation at 5,000 x g for 10 min, and DNA was precipitated with a 1:10 volume of 3 M sodium acetate, pH 4.7, and a 2.5 volume of cold 100% ethanol. After 30 min of incubation at –80 ºC, the DNA was sedimented by centrifugation at 12,000 x g for 15 min. The DNA was washed twice with cold 70% ethanol and dried before resuspension in buffer (10 mM Tris-HCl, pH 8.0, 1 mM EDTA, pH 8.0). The DNA was subject to 1% gel electrophoresis and then stored at –4º C.

2.5 Trypanosoma cruzi and Leishmania brasiliensis Nuclear DNA (nDNA)

The *T. cruzi* epimastigote and the *L. brasiliensis* promastigote were collected by centrifugation at 3,000 x g for 15 min. The pellets were washed twice in TBS (5 x 10^7 flagellates/mL) and were resuspended in the extraction buffer. After a period of 1 h at 37 ºC, proteinase-K (100 µg/mL) was added, and the incubation proceeded for 12 h, following the same steps as those of the host cells.

2.6 *Trypanosoma cruzi* Mitochondrion DNA (kDNA)

kDNA was extracted from *T. cruzi* and from *L. brasiliensis*. In brief, either 5 x 10^7 epimastigotes or equal quantities of promastigotes were washed three times in PBS, collected by centrifugation, and resuspended in 630 µL of NET buffer (10 mM Tris HCL,100 mM EDTA, 100 mM NaCl, pH 8.0). The cells underwent lysis with the addition of 70 µL of 10% SDS and 7 µL of 20 mg/mL proteinase-K. After incubation for an additional 12 h the lysate was homogenized by sheering, and 690 µL of NET buffer with 100 µL 20% sucrose was added. The mix was centrifuged at 14,000 x g for 15 min, and the supernatant removed with a pipette tip. The remaining 30 µL was resuspended in NET buffer containing sucrose. The pellet was collected by centrifugation, resuspended in 100 µL of distilled water, and subjected to subsequent extractions as described for the host cells. The kDNA was precipitated with 2.5 volumes of 100% ethanol and 0.1 volume of 3 M sodium acetate, pH 8.0. The pellet was washed twice with 70% ethanol, and the kDNA resuspended in 200 µL of TE buffer and stored at 4 ºC.

2.7 Quantification, Enzyme Digestion and Electrophoretic Analysis of DNA

The DNA samples was quantified by the spectrophotometric method, and the integrity and purity demonstrated by 1% gel electrophoresis in TAE buffer (90 mM Tris-acetate, pH 8.0, 25 mM EDTA). The digestion of the DNA was carried out by restriction enzyme, and 2 units of *Eco*R1 cut 1µg of DNA. After 4 h of incubation, the DNA fragments that were separated by gel electrophoresis were excised from the gel and purified.

2.8 Southern Blot

The purified DNA fragments were separated by electrophoresis in a 1% agarose gel and transferred by the alkaline capillarity method to the nylon membrane in a denaturing solution (0.4 M NaOH). After transfer, the DNA was dried out and fixed to the membrane at room temperature.

The probes were radio labeled by the Random Primer Labeling System via the insertion of [α-^{32}P]-dATP in the DNA sequence synthesis with Klenow polymerase in the presence of hexamer random primers [45]. The radiolabeled probes were purified by chromatography in a Sephadex G-10 column, and the radioactivity confirmed by scintigraphy showed >10^8 counts/µg of the DNA. Membrane prehybridization was caried out for 4 h at 65 ºC in 0.5% SDS, 5X Denhardt solution with 100 µg salmon DNA.

2.9 PCR Amplifications and Hybridizations

The *T. cruzi* kDNA amplification with the specific primer sets S34/37 and S35/36 secured the kinetoplast minicircle sequence [46]. The internal oligonucleotide constant region amplification was obtained from the *T. cruzi* kDNA, using primers S34 and S67, and the nested S35 antisense primer. The 330-bp kinetoplast minicircle constant region kCR probe was PCR-amplified from the *T. cruzi*-infected host cell DNA template with the primers S34/S67, cloned into the TA vector, and sequenced. The primer set S34/37 amplified as little as 15 fg of conserved and variable sequence of the kDNA minicircle from *T. cruzi*-infected host cells [23]. The *T. cruzi* telomere DNA (nDNA) 188 nt sequence probe was PCR amplified with Tcz1/Tcz2 primers and validated by Southern blot with radio labeled nCR probe. The primer sets Tcz1/Tcz2 amplified as little as 10 fg of *T. cruzi* nDNA repetitive telomere sequences [47]. The kDNA and nDNA specific primers and probes are shown in Tables 1 and 2.

Table 1 The *Trypanosoma cruzi* kinetoplast DNA and nuclear DNA primers

	Target	**Sequence**
kDNA		
S34	kDNA	ACA CCA ACC CCA ATC GAA CC
S67	kDNA	GGT TTT GGG AGG GG(G/C) (G/C)(T/G)TC
S35	kDNA	ATA ATG TAC GGG (T/G)GA GAT GC
S35 reverse	kDNA	GCA TCT CMC CCG TAC ATT AT
S67 reverse	kDNA	GAM SSC CCC TCC CAA AACC
S36	kDNA	GGT TCG ATT GGG GTT GGT G
nDNA		
Tcz1	Telomere	5’ GAG CTC TTG CCC CAC ACG GGT GCT 3’
Tcz2	Telomere	5’ CCT CCA AGC AGC GGA TAG TTC ACG 3’

The *T. cruzi* nCR and kCR sequences with annealing nucleotides underlined, were employed for hybridization. The PCR assays were conducted with a template DNA concentration 20-fold above the levels of detection, with 10 ng of each pair of primers, 0.5 IU of *Taq,* and 0.2 mM of each dNTP in a final volume 25 µL. The kCR and the nCR probe radio label [α-^{32}P]-dATP showed specific activity of three thousand ci/mM and maximum stringency 0.1% SSC and 0.1 SDS, at 65 ºC for 1 h.

Table 2 The *Trypanosoma cruzi* nucleus and kinetoplast DNA-derived probe sequences, with primer binding sites underlined

Probe	Sequence
nCR	
Nucleus Telomere	5' CGAGCTCTTGCCCACACGGGTGCTGCACTCGGCTGATCGTTTTCGAG CGCTGCT GCATCACACGTCCAAATTTTTGTTTCCCGATTGTGAATGG TGGGAGTCAGAGGCACTCTCTGTCAATATCTGTTTGCGTGTTCACACACTGGACACCAAACAACCCTGAA CTATCCGCTTGGA GGA ATTCG3'
kCR	
Kinetoplast minicircle	5' TTTTGGTTTTGGTGGGAGGGGGCGTTCA AATTTTGGCCGAAAATTCATGCATCTCCCCCTACATTATTGGCCGAAAATGGGGGTTGTTCGAG GTGAGGTTCGATTGGGTGGTGTAAG 3'

The *T. cruzi* kDNA probe showed specific hybridization with the cloned kDNA minicircle in phage m13mp8, but it did not hybridize with genes in plasmids pTC4, PTC1 and PK03 [48, 49]. The amplicons were obtained with 200 ng of test DNA template and 10 ng of each primer set in the Reaction Buffer (50 mM KCl, 10 mM Tris HCL, pH 9.0, 1.5 mM $MgCl_2$, 0.2 mM dNTPs and 2.5 units of *Taq*-polymerase). *T. cruzi* and *L. brasiliensis* DNA were used as controls. The PCRs were conducted in agreement with a previous work [45]. The bands in the gels were transferred to nylon membranes and hybridized with radio labeled specific probes. The sensitivity of the PCR with the primer sets Tcz1/Tcz2 was tested with serial dilutions of the *T. cruzi* nDNA highly repetitive telomere sequence.

2.10 Amplification of the integrated kDNA Minicircle Sequence

The method for amplification of kDNA minicircle sequence integration into genomic flanking regions used the kDNA primer sets in either a 5'-3'or 3'-5' combination. The fragments obtained by PCR amplifications from *T. cruzi*-infected rabbit tissues that hybridized with the radiolabeled specific kCR probe were characterized by sequencing.

Second, a targeting primer thermal asymmetric interlaced-PCR (*tp*TAIL-PCR) method was used to amplify LINE-1 from the genomes of chickens and mice with specific primers combined with the successive kDNA minicircle internal primers. The LINE-1 primer concentration was 10-fold below that of the kDNA primers employed. The primers anneal to a gamut of contigs to amplify the transposon families [45, 50].

2.11 Rabbit Model

Two-month-old male and female New Zealand white rabbits were fed pellet chow and water *ad libitum* and housed in individual cages at 65% humidity and a temperature 24 ºC in the animal room. The rabbits of groups A and B were inoculated subcutaneously with 2.5 x 10^6 *T. cruzi* trypomastigotes collected from the muscle cell cultures. The group C were uninfected controls. The *T. cruzi*-infected group A rabbits were untreated. The therapeutic effect of the nitro-heterocycle benznidazole was investigated in eight rabbits of the group B. The *T. cruzi*-infected rabbits in group B were treated with intraperitoneal injections of benznidazole (8 mg/kg body weight) for 60 days. The rabbits of groups A and B, and uninfected control group C were subjected to clinical inspections for heart disease, and necropsy. The tissues fixed in 5% formalin were embedded in paraffin, cut 5 µm thin sections, hematoxylin-eosin (H-E) staining and histopathological analysis.

2.12 Inoculation of Naked kDNA in Rabbits and in Fertile Chicken Eggs

Four 60 day-old-old rabbits were injected with 375 µg of kDNA minicircles or with 125 µg of a cloned kDNA sequence (GeneBank accession number AF399842). In addition, 30 fertile eggs received 15 ng of minicircles or 5 ng of cloned kDNA in the air chamber. The presence of kDNA in tissues was assayed by PCR.

2.13 Chicken Model

In this investigation, white Ross fertile chicken eggs were infected with 100 *T. cruzi* trypomastigotes through a hole made in the eggshell air chamber and sealed with adhesive tape. The mock control eggs received culture medium, only. These eggs hatched after 21-day incubation in a chamber at 37 ºC, with 65% humidity, while rolling for a few seconds every two hours; this incubation occurred in a chicken room maintained at an average 24 ºC, under positive pressure

with filtered air and exhaust. The chicks hatched in the incubator and remained there for 24 h and, thereafter, at 32 º C for one month and grew to adulthood. In addition, F0 hens fertilized by artificial insemination laid eggs that hatched F1 chicks, and the repeat insemination of adult F1 chicken generated F2 chicks. The F0, F1, and F2 chickens were used in the experiments. We observed that the embryonic stem cell cultures from uninfected control chicken blast cells erupted from the zygote membrane six hours after the egg incubation. The embryo blast cells adhered to the plastic surface and grew at 37 ºC and 65% humidity upon infection with *β*-galactosidase-expressing *T. cruzi* trypomastigotes [45, 50].

The DNA analysis was conducted with peripheral blood mononuclear cells and solid tissues from forty-eight chickens that hatched from eggs inoculated with 100 *T. cruzi* forms, and from mock control chickens. These flocks grew to adulthoods in individual cages and were fed commercial chow and water *ad libitum.*

2.13.1 DNA Extraction and Nucleic Acids Analyses

We extracted semen from roosters, from the embryo tissues of non-inseminated eggs at set points of incubation, from tissues of chickens hatched from *T. cruzi*-inoculated eggs, and from mock controls. Here, DNAs from the semen, heart, skeletal muscle, and large bowel of *T. cruzi* inoculated eggs, and from mock control chickens, was employed. These genomic DNA samples were templates for PCR amplification performed in triplicate. The nCR and kCR amplicons were resolved in 1.3% agarose gel, transferred to a nylon membrane, and hybridized with a specific [μ^{32}P]-dATP-radio labeled probe. A random primer labeling kit was employed to label the nCR and kCR probes.

Southern hybridization of DNA from the *T. cruzi*-infected, from mock control eggs, and from *T. cruzi* kDNA positive control was performed in agreement with protocols described elsewhere [13]. The *tp*TAIL-PCR was conducted with kDNA primer sets s34/s67, s35/s35as, and s67as/s36, respectively, through three cycles of the reaction each in combination with each chicken primer Gg1 to Gg6, and with XeCrs1 to XeCrs2 (Table 3). The product obtained during each cycle was validated by Southern blot with the radio labeled kCR probe and subjected to clone and sequence.

Table 3 *Gallus gallus* DNA primers used in PCR amplification

Primer	Sequence	Tm*
Gg1	5’ AGA GAA CTG CTT GAA ACC TAC AGG 3’	60.1
Gg2	5’ GTG AAA GGC CTA TAT CAA GTC AGC 3’	56.8
Gg3	5’ CCA AGG AGC TGG TAG AGA GCA 3’	60.1
Gg4	5’ CCA CGC TGG GAG AAG AGT T 3’	64.2
Gg5	5’ CTC ACT TCC TCC CTT CCC A 3’	62.3
Gg6	5’ CTG TTA GCA TGA GGC TTC ACA A 3’	60.4
XeCRs1	5’ ATW TCW GTS TTT GCA GAT GAC ACA 3’	60.4
XeCRs2	5’ CTT WGT TGC CCT YCT CTG KAC YCT CTC YA 3’	60.4
XeCRs3	5’ TGT GTC ATC TGC AAA SAC WGA WAT 3’	66.6
XeCRS4	5’TRG AGA GRG TMC AGA GRA GGG CAA CWA TG 3’	65.3
XeCRs5	5’TRG AGA GRG TMC AGA GRA GGG CAA CWA 3’	67.9

The primers anneal to a specific region of the chimera sequence (GB FN599618) in the *locus* NW_001471673.1 on chromosome 3. These primers at a 0.004 µM concentration and their annealing temperature were used in combination with kDNA primers. Those clones showing hybridization with radio labeled kDNA were sequenced. The *tp*TAIL-PCR was validated in a mix of *T. cruzi* kDNA with DNA from naïve control birds.

2.13.2 Heart Protein Extraction and 2DE Identification

Heart tissue samples were obtained from kDNA+ and kDNA- adult chickens. The myocardium was minced, washed with a protein inhibitor cocktail in PBS (5 mm EDTA, 100 µM PMSF, 100 µM TLCK, 100 µM TPCK, 1 µM pepstatin, 100 µM leupeptin) at 4 ºC, and centrifuged at 10,000 rpm. The pellet was resuspended in lysis buffer (7 M urea, 2M thiourea, 2% Triton X-100, 1% DTT and the protease inhibitor cocktail). The protein profiles of heart extracts (100 µg) that were

analyzed by two-dimension (2DE) electrophoresis, then, were subjected to Peptide mass fingerprinting for protein identification using a mass spectrometer. The electrophoretic transfer of proteins from polyacrylamide gels to sheet of nitrocellulose membrane were made, followed by immunodetection of heart antigen with peroxidase labeled anti-chicken antibody.

2.13.3 Chagas Disease clinical and pathological findings

Clinical parameters in the chickens hatched from *T. cruzi*-infected eggs (kDNA+) and in the healthy controls (kDNA-) were detected by inspection and by arrhythmias and increasing heart size by electrocardiography (ECG) recordings. A one-channel ECG apparatus with standard 1 mV/cm and speed of 25 min/sec was used with the electrodes under the wing pits and on the back of the legs. ECG recordings of frontal leads AVR, AVL, and AVF, and assessment of mean electrical axis deviation to the left, were obtained. These experiments were carried out with 35 kDNA+ and with 22 kDNA- chickens. After death, each chicken was subjected to necropsy and the heart weight recorded. The tissues fixed in formalin, embedded in paraffin, were cut 5 µm sections and H-E stained for histopathology.

2.14 Mouse Model

Groups of 8-two-month-old BALB/c, male and female, mice weighing 20 to 25 grams were separately housed in cages maintained at 24 ºC, and 65% humidity, under pressure air exhaust, and fed commercial pellets and water *ad libitum*. The mice in the experimental groups received intraperitoneal inoculations with 10 x 10^3 *T. cruzi* trypomastigotes harvested from L6 muscle cell cultures. The parasitemia in the *T. cruzi*-infected mice was determined by direct microscopic examination of the tail-blood under cover slip on a Neubauer cell counting. The blood samples were collected at the 5th day post-infection and thereafter every 15 days until the 60th day. In addition, the demonstration of *T. cruzi* in the blood was secured by hemoculture in a screwcap glass culture tube containing 5 mL of blood-agar slant plus 5 mL of LIT medium overlay. These culture tubes were inoculated with 100 µL of blood drawn by heart puncture from *T. cruzi*-infected mice, and kept in a shaker incubator at 27 ºC, during a period of 60 days. The cultures examined by microscopy at 20, 40 and 60th day.

Tissue samples of *T. cruzi*-infected mice in the A, B, and C groups had their body tissue subjected to DNA extraction, and samples fixed in formalin were subjected to histopathology. These procedures searched for tissue lesions in *T. cruzi*-infected mice treated with drug inhibitors of eukaryotic cell growth and differentiation, and in mock controls mice.

2.14.1 Multi-Drug Treatment of the T. cruzi-Infected Mice

Table 4 Checkpoint inhibitors of cell growth and differentiation

Drug inhibitor	**Activity**	**Dose (µM)**	**References**
		Cell growth inhibition	
Azido-thymidine	Intercalating thymidine in the DNA inhibits reverse transcription at G2/M phase, caspase-3- induced cell division inhibition, and apoptosis.	0.13	51
Bromo-deoxyuridine	Intercalating Br-uridine at S phase stops cell cycle and cell growth.	0.09	52
Colchicine	Suppression of tubulin assembly inhibits microtubule dependent cell division.	0.12	53
Genistein	ATP inhibition through protein Tyrosine kinase (PTK) and cell growth.	0.037	54
Microcystin LR	Inhibits PP1 and PP2 serine/threonine phosphatases and cell growth.	0.005	55
			56
Mitomycin-C	Inhibits PP1 and PP2 serine/threonine/ Phosphatases.	0.02	57
		Polymerase inhibitors	
Camptothecin	Downregulates S phase checkpoint by ATR/CHK1 Polymerase I (DNA gyrase).	0.14	58

Cycloheximide	Inhibits p38-activated protein kinase (MAKPK) and entry at G2/M mitotic phase.	0.17	59
Etoposide	Downregulates polymerase II at S-G2 phases and prevents cell division.	0.08	60
Ofloxacin*	4-Fluoroquinolone affects polymerase II metabolic pathway at G2/M phase and apoptosis.	0.083	61
			62
Praziquantel	Inhibits protein serine/threonine kinase (PI3-k) and polymerases I and II.	0.147	63
Staurosporine	Protein kinases (A, C, CAM and PI3K) inhibitor prevents cell growth at G1 checkpoint.	0.19	64
			65

Groups of eight, two-month-old BALB/c mice were used for the multidrug treatment of *T. cruzi* infection. Each mouse in groups A to H received intraperitoneal inoculation of 10^4 *T. cruzi* trypomastigotes derived from L6 muscle cell cultures. Mice in group A), were positive control, *T. cruzi*-infected, untreated. *T. cruzi*-infected mice in groups B to G received 0.86 mg benznidazole daily. In addition to benznidazole, each mouse group received an inhibitor of eukaryote cell growth: azidothymidine, group C; ofloxacin group D; and praziquantel, group E. Group A, was the control and received no inhibitor. Additionally, a multidrug regimen was administered to the following mice groups: F) ofloxacin and azidothymidine. G) ofloxacin and praziquantel. H) Azido thymidine, and praziquantel. DNA from *L. brasiliensis* and from uninfected mice were negative controls. DNA from *T. cruzi* was the positive control. The daily drug administration regimen was initiated at the fifth day post-infection and continued for 60 days. Each drug powder stock was suspended in distilled water to the concentration indicated in Table 4, and the aliquot mix was administered through gavage using a 4 cm long urethral catheter nº 3.

2.14.2 Detection of Parasitemia

The parasitemia in *T. cruzi*-infected mice was determined by examination of the flagellates in a drop of tail-collected blood at the 5th day post-infection and thereafter every 15 days until the 60th day. The parasite counts in 5 *u*L of blood diluted sample 1:2 under a 2 x 2 coverslip on a hemocytometer were determined by microscopy. Additionally, the presence of late-phase parasites was determined by hemoculture of 100 *u*L of blood collected through heart puncture at 20-, 40- and 60-days post-infection. The mortality of mice in the A-to-H groups was recorded and the deceased were subjected to necropsy and had their tissue samples subjected to DNA extraction and fixed in formalin to histopathology. The mice were sacrificed under anesthesia at the end of experiments at the 250th day of infection.

2.14.3 Detection of Serum T. cruzi Antibody

The *T. cruzi* antibody titers were revealed by the enzyme-linked immunosorbent assay (ELISA) as described elsewhere [66]. A spectrophotometer was used for plate reading at a wavelength of 480 nm. The optical density above a 0.064 cut-off separated positive from negative antibody reactions.

2.14.4 Extraction of DNA from Trypanosoma cruzi-Infected, Infected-Treated, and from Control Uninfected Mice

At the 250th -day-end experiment the tissue samples from the heart, skeletal muscle, large intestine, and spleen from each mouse were collected. Small fragments (approximately 200 mg) of each tissue were transferred to sterile dishes were minced and transferred to sterile 15 mL screw-cap plastic tubes. DNA extraction from these samples was carried out stepwise according with description in section 4.1. The PCR protocol for the nucleic acid-based diagnosis of *T. cruzi* infection with exact methods to identify the *T. cruzi* nuclear DNA (nDNA) in the tissues is described elsewhere [13].

2.14.5 Targeting Primer Thermal Asymmetric Interlaced PCR

The specific site of the kDNA minicircle sequence integration into the human genome was identified by the *tp*TAIL-PCR [13]. The study showed that 70.8% of the kDNA integrations occurred in retrotransposon LINE-1. Interestingly, the kDNA minicircle sequence integrated into the chicken CR-1 transposon [67]. This information led to unraveling the *T. cruzi* integration sites into retrotransposon LINE families in the mouse genome. The primers employed in the reactions are shown in Table 5.

Table 5 *Mus musculus* LINE-1 specific primers

Primer	Target	Family	Sequence (5'→3')
L1cam – 5' UTR F Sense	5' UTR	F	ACC TTC CCT GTA AGA GGA GAG
L1cam – 5' UTR F Antisense	5' UTR	F	GCT CTC CTC TTA CAG GGA AGG T
L1cam – 5' UTR A Sense	5' UTR	A	GAC CTC TGG TGA GTG GAT CAC
L1cam – 5' UTR A Antisense	5' UTR	A	GTG ATC CAC TCA CCA GAG GTC
L1cam – 5' UTR T_F Sense	5' UTR	T_F	TTA GTC TGA ACA GGT GAG AGG
L1cam – 5' UTR T_F Antisense	5' UTR	T_F	CCT CTC ACC TGT TCA GAC TAA
L1cam – 5' UTR G_F Sense	5' UTR	G_F	GCG CCA TCT TCA GCT CCA GA
L1cam – 5' UTR G_F Antisense	5' UTR	G_F	TCT GGA GCT GAA GAT GGC GC
L1 cam – 2	ORF 1	All	CTA TGA AAG CCA GAA GAG CCT G
L1 cam – 3	ORF 2	All	ACA GCC ACA AGA ACA GAA TGC
L1 cam – 4	3' UTR	All	GCC TAG TCG GCC ATC ACT G
L1 cam – 5 (L1 cam 4 Antisense)	3' UTR	All	CAG TGA TGG CCG ACT AGG C
L1 cam – 6 (L1 cam 3 Antisense)	ORF 2	All	GCA TTC TGT TCT TGT GGC TGT
L1 cam – 7 (L1 cam 2 Antisense)	ORF 1	All	CAG GCT CTT CTG GCT TTC ATA G
ORF2(01) Sense	ORF 2	All	GAG TGC CTC CAA GAA GAA ACG
ORF2(01) Antisense	ORF 2	All	CGT TTC TTC TTG GAG GCA CTC
ORF2(02) Sense	ORF 2	All	TCA TCC ATC CTG ACC AAG TAG G
ORF2(02) Antisense	ORF 2	All	CCT ACT TGG TCA GGA TGG TGA

Table 6 Temperature set for *tp*TAIL-PCR amplification*

Cycle I				**Cycle II**				**Cycle III**			
Step 1	1×	94 °C	5 min	Step 1	1×	94 °C	5 min	Step 1	1×	94 °C	5 min
Step 2	5×	94 °C	30 s	Step 2	12×	94 °C	30 s	Step 2	20×	94 °C	30 s
		64 °C	1 min			64 °C	1 min			45 °C	1 min
		72 °C	2 min			72 °C	2 min			72 °C	2 min
Step 3	1×	94 °C	30 s			94 °C	30 s	Step 3	1×	72 °C	7 min
		25 °C	1 min			64 °C	1 min	Step 4		4 °C	∞
		72 °C	2 min			72 °C	2 min				
Step 4	12×	94 °C	30 s			94 °C	30 s				
		64 °C	1 min			45 °C	1 min				
		72 °C	2 min			72 °C	2 min				
		94 °C	30 s	Step 3	1×	72 °C	7 min				
		64 °C	1 min	Step 4		4 °C	∞				
		72 °C	2 min								
		94 °C	30 s								
		44 °C	1 min								
		72 °C	2 min								
Step 5	1×	72 °C	7 min								
Step 6		4 °C	∞								

*Average temperature ºC.

The *tp*TAIL-PCR employed the kDNA primer sets, each in combination with a primer specific to the mouse LINE, throughout three cycles of the reaction programmed at set temperature showed in Table 6.

The mouse DNA samples were amplified after each reaction cycle initiated by the kDNA minicircle sequence primer combined with the mouse LINE retrotransposon-specific primer. The *tp*TAIL-PCR scheme covered the LINE 5' short direct repeat (SDR), the 3' and 5' untranslated regions (UTR), the open reading frames (ORF1 and ORF2), and the poli-A tail (An) of LINE-1. In addition, the conserved sequence block (CSB) conserved and variable regions, kDNA minicircle sequence amplification, and mouse LINE DNA shown in Figure 1.

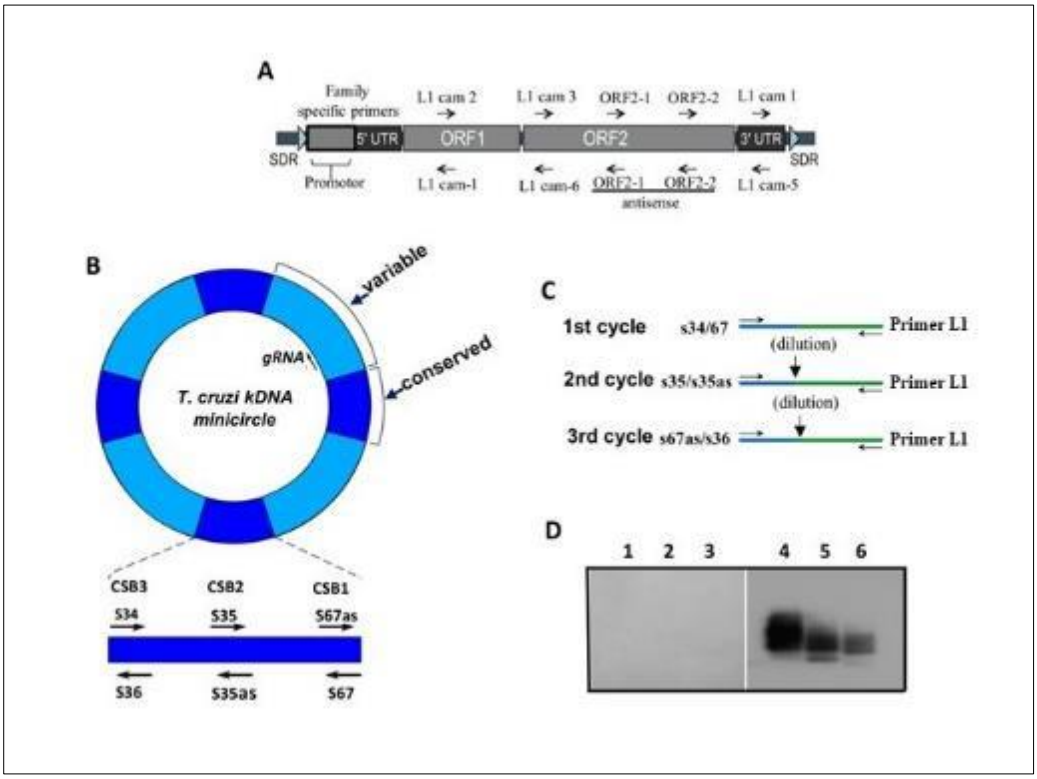

Figure 1 Schematic representation of the *tp*TAIL-PCR amplification of *Trypanosoma cruzi* minicircle integrated into the mouse genome

Panel A) Obtaining integrated kDNA minicircle sequence after three cycles of amplifications. The scheme depicted the *Mus musculus* retrotransposon LINE-1 cam element (gray) and the array of primers (arrows) used in the reaction.

Panel B). Amplification of minicircle constant and variable sequences. The *T. cruzi* kDNA minicircle showing the constant (light blue) and the variable (dark blue) interspersed regions, a straight demonstration of the CSBs 3, CSB2, and CSB1. Primers anneal (arrows) downstream and upstream amplify constant and variable sequence comprising 300 nucleotides.

Panel C). Reamplification cycles used during the *tp*TAIL-PCR reaction. Notice that each amplification cycle employed the previous cycle amplification product for the subsequent amplification using the kDNA internal primer in combination with the LINE-1 primer.

Panel D). Validation of the *tp*TAIL-PCR products after each of three cycles of amplification. The products obtained after each PCR amplification cycle was separated in agarose gel 0.7%, and Southern blot with a *T. cruzi*-specific minicircle constant region radio labeled kCR probe, clone, and sequence. Lanes 1 to 3, control, uninfected mouse DNA. Lanes 4, 5, and 6, products of *T. cruzi*-infected mouse DNA.

2.14.6 Southern Blot and Radio Labeled Probe Hybridization

The *tp*TAIL-PCR-amplified sequences were separated by electrophoresis in a 1% agarose gel and transferred to a positively charged nylon membrane by the alkaline transfer method. The *T. cruzi* kDNA probe (kCR) was subjected to [α-^{32}P] -dATP labeling reaction with triphosphate deoxynucleotides dATP, dCTP, dGTP and dTTP (20 µM), three units of the Klenow DNA-polymerase-I, 15.0 µL of random primer buffer mixture, and 5 µL of radio labeled dATP at 3,000 µCi activity. The reaction took place for 3 h and the radio-labeled kCR probe was purified in a Sephadex G25 column.

The DNA immobilized on the nylon membrane had positive charges blocked with a pre-hybridization solution (10% PEG 800, 7% SDS, 1.5% SSPE, 100 µg/mL salmon sperm) at 65 ºC for 15 min. The membranes were then inserted into a cassette for film exposure to X-rays and stored at –80 ºC for 7 to 10 days. The films were washed with developing and fixation solutions in the dark to reveal the DNA bands.

2.14.7 Cloning and Sequencing

The DNA sequences were determined after the third *tp*TAIL-PCR amplification cycle. Each mouse DNA sample were subdivided into eight aliquots and the amplification products from each *tp*TAIL-PCR third cycle from four repeat runs were ligated by T4 ligase into the pGEM T-Easy Vector at 4 ºC for 12 h. Competent *Escherichia coli* X10-Gold cells were treated with rubidium chloride and transformed by thermal shock. The cells were inoculated in Luria Bertani (LB) broth at 37 ºC for 3 h to achieve maximal growth at OD 600. The broth was then centrifuged, and the cells transferred to Petri dish to grow on LB agar with 4.8 x 10^{-2} µg/mL X-Gal and 0.1 µg/µL ampicillin.

Recombinant ampicillin resistant white colonies that grew on nylon membranes were treated for hybridization with a radio labeled kCR probe. The recombinants showing intense hybridization were selected for plasmid extraction. The inserts were released by *Eco*RI enzyme digestion, and those showing strong hybridization signals selected for commercial sequencing. Four rounds of the *tp*TAIL-PCR three-cycle amplification yielded selection of the nonredundant sequences from the DNA of each group of mice.

2.14.8 Sequence Analysis

The sequences were analyzed for similarity with those from *Mus musculus* and from *Trypanosoma cruzi* retrieved from the GenBank/NCBI. The nonredundant nucleotides searches were conducted throughout the GenBank/EMBL/DDBJ and RefSeqs databases. The Blastn version 2.2.25 parameters used were e-threshold: 10; and word size 11. The scores used as thresholds were as follows: match/mismatch 1, -2; gap costs, existence 5 and extension 2. The repeat masker CENSOR was used to map the sequences, and the repeats classification was obtained by alignment with those in the LINEs families A, T_F, and G_F. The reference sequences L1Md-A2 (M13002.1) for family A, L1spa (AF016099.1) for family T_F, and L1Md-GF62 (MG1:2178803) for family G_F.

2.14.9 Statistics

One-way ANOVA-F employed for the statistical analysis and evaluation of the distributions of the kDNA mutations among the experimental data. Student's *t* test was used to detect differences between uninfected control and kDNA mutated chicken progeny (FO to F2), and between kDNA mutation indexes in groups of *T. cruzi*-infected treated and untreated mice, and the control uninfected groups.

2.14.10 Histopathology

The tissues from the mice of groups A to H were washed with 1X, PBS pH 7.2, fixed in 4% formaldehyde solution for 72 h., cut 5µ thin sections and subjected to histopathological analysis.

3 Results

3.1 Rabbit Model

It has been observed that the treatment of chronically *T. cruzi*-infected humans with a trypanosome-killing agent neither stop the parasitemia nor the progressively destructive myocarditis and peripheral nerve system ganglionitis, hallmarks of Chagas disease [67-73]. What could be sustaining active destruction of the heart cells? To answer this question, it was postulated that a steady rate of genetic transfer could occur from the parasite to the host genome and that resulting mutation could explain the autoimmune rejection of tissues of Chagas disease patients [72, 73]. Genomic DNA samples from the blood of 13 Chagas heart disease patients who had shown antibodies specific to *T. cruzi* and had manifested the clinical symptoms of chronic Chagas heart disease were analyzed. These samples harbored parasite DNA as judged by PCR amplification with primers for both *T. cruzi* nDNA and kDNA minicircles (Figure 2). Southern hybridization was conducted on genomic DNA from these Chagas patients. In a typical example, the DNA sample from Chagas patient 245 revealed 400 and 100 bp bands with the kDNA minicircle probe only, whereas digested and catenated minicircles revealed high molecular weight bands of 1.4 kb and larger, respectively (Figure 2).

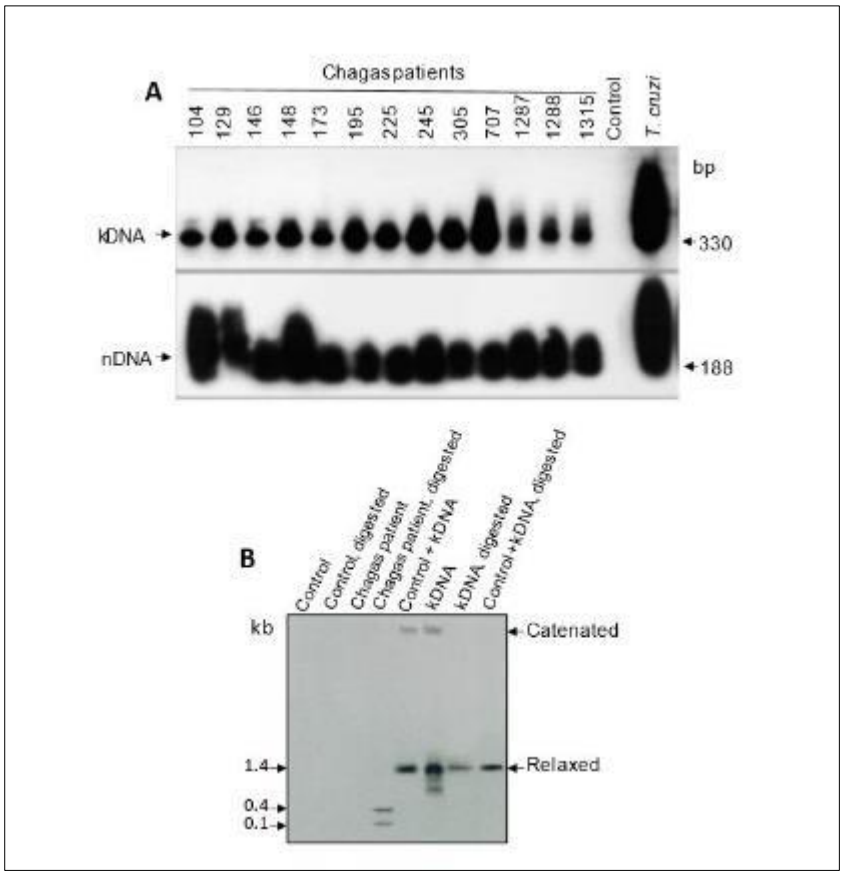

Figure 2 Genetic markers of *T. cruzi* DNA in chronic Chagas patients

Panel A). PCR amplification of kDNA and nDNA from blood cells of chronically *T. cruzi*-infected humans. DNA template product obtained from 13 Chagas heart disease patients and specific sets of kDNA (S35/S36; upper panel) and nDNA (Tcz1/Tcz2; lower panel primers) which hybridized with specific internal probes S67 and Tcz3, respectively, on blots of 1% agarose gels. The size markers indicate the minimal unit size of amplification in each case.

Panel B. Southern hybridization of integrated kDNA revealed by a minicircle sequence (kCR) probe. A 0.7% agarose gel was used to analyze undigested DNA or *Eco*R1 *and Bam*HI double- digested DNA from the blood of Chagas disease patient 245. After size separation through a 0.7% agarose gel, the DNA was stained with ethidium bromide, blotted, and probed with the kCR oligonucleotide. DNA from a noninfected human donor and purified kDNA were included as controls. The predicted sizes of catenated and relaxed or linear minicircle are indicated.

The ongoing process of genetic transfer between *T. cruzi* and rabbit was investigated with the examination of DNA from tissues extracted from eight animals that had been infected for six months to three years. *Bam*H1 digests of DNA extracted from blood, heart, skeletal muscle, liver, intestine, and kidney were hybridized with the kCR probe anneal to *T. cruzi* kDNA minicircle. A 2.2 kb band was obtained with the heart- and intestine-derived DNA samples, distinct from the minicircle unit-sized 1.4 kb band hybridizing in parasite DNA alone. DNA extracted from tissues of uninfected rabbit showed no hybridization with the kCR probe. The tissue samples showed no hybridization with the other *T. cruzi*-specific nDNA probes for high-copy number genes repetitive sequences (Figure 3).

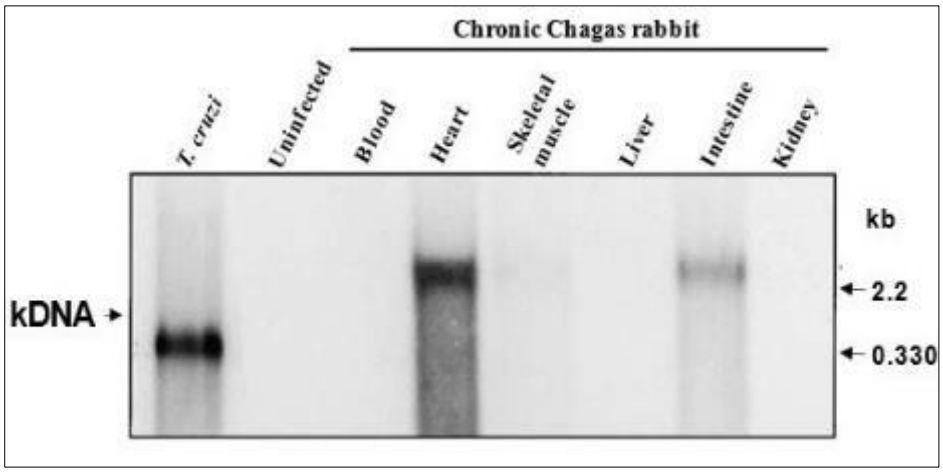

Figure 3 Southern blot showing the integration of kDNA minicircle into the genome of a Chagas disease rabbit

Integration of kDNA minicircle sequence into a transposable element in the genome of a *T. cruzi*-infected rabbit. PCR amplification of rabbit DNA specific with primers S34/S35 and kCR kDNA probe. EcoR1 digested DNA (20 *u*g) separated in 0.7% agarose gel was used for Southern hybridization with 1 *u*g of *T. cruzi* kinetoplast kCR probe. The *T. cruzi* DNA formed a 0.330 kb band of kDNA minicircle sequence, whereas the rabbit heart and intestine DNA yielded a 2.2 kb band thus, suggesting that the kDNA minicircle was integrated into the genome.

To characterize the 2.2 kb band, PCR with the kDNA direct and reverse primers (Table 1) was employed on DNA from infected rabbit hearts. This approach generated sequences containing both arms of rabbit DNA flanking the kDNA insertion (GenBank AY488498 to AY488503, AF399841, AF400668, and AF415293). Integration of a CCA/ACC rich kDNA fragment (bp 1255-1907) occurred at attachment sites of direct CACCAACC repeats within the rabbit DNA (Figure 3 and S2 Table), thus indicating the kDNA minicircle sequence integrations were mediated by nonhomologous end-joining recombination.

The de novo transfer of kDNA to the rabbit genome occurred during the normal course of infection. The kDNA integration sites introduced modification in the human genome could represent a critical biological feature in host-pathogen interaction and clinical manifestation of Chagas disease. Inoculation of kDNA sequences did not yield integrations of the exogenous minicircle into the rabbit genome.

To further dissect the process of genetic transfer from *T. cruzi* to Chagas patients, we continued the studies into rabbits amenable to the Protist infection.

3.1.1 Trypanosoma cruzi Infection of Rabbits, Treatment with Nitro-Heterocycle Benznidazole, and Pathology

We performed experiments in groups of *T. cruzi*-infected rabbits to determine whether the administration of the benznidazole could halt the transfer of kDNA and Chagas heart disease pathology. Three groups of eight two-month-old male and female rabbits were housed in individual cages. The uninfected-control group A rabbits (Figure 4). were *T. cruzi* antibody-free.

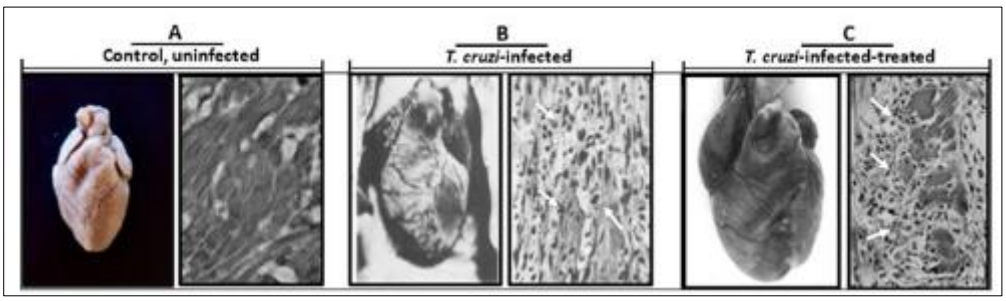

Figure 4 The heart pathology in *T. cruzi*-infected rabbits

Panel A). Control, normal heart size (15 g) and histology from an 18-month-old New Zealand white rabbit.

Panel B). Cardiomegaly (25 g) from a 15-month-old, *T. cruzi*-infected New Zealand white rabbit. Notice the cardiomyopathy with dilation of the right atrium and ventricle, and of the left ventricle. The histopathology showed mononuclear cells infiltration and lysis (minimal rejection units, arrows) of parasite-free target heart cells.

Panel C). Cardiomegaly (30 g) from an 18-month-old *T. cruzi*-infected -treated New Zealand white rabbit. Notice the cardiomyopathy with dilation of the right atrium and ventricle. The histopathology showed mononuclear cells infiltration and lysis (minimal rejection units, arrows) of parasite free heart cells.

The rabbits' groups B and C were each inoculated subcutaneously with 2.5 x 10^6 *T. cruzi* trypomastigotes. The drug powder (8 mg/ml suspension in 0.15 M saline) was administered to the *T. cruzi*-infected rabbits groups B and C (8mg/kg body weight) during a period range from the 40th day to the 100th day post-infection (Figure 4). The *T. cruzi*-infected-untreated (group B) and the *T. cruzi*-infected- treated rabbits (group C) showed ELISA-specific antibody titers throughout the long-lasting infections.

In the late chronic infection rabbits of groups, B and C showed cyanosis, shortness of breath and ascites. The heart pathology of *T. cruzi*-infected rabbits either untreated (group B) or benznidazole-treated (group C) showed cardiomegaly with dilation of the atria and the ventricles. The histopathology revealed lymphocyte-lysed target cells. The severe myocarditis in the groups B rabbits was qualitatively like that seen in the benznidazole treated-*T. cruzi*-infected- group C rabbits (Figure 4 B and C). Tissue-specific lymphocyte-lysed target cells lesion in muscle tissues, which usually extended to the peripheral nervous systems of stillborn offspring of *T. cruzi*-infected rabbits, were observed in the rabbit model system. None of these lesions were seen in any tissue of control, uninfected rabbits (Figure 4A).

3.1.2 Integration of Trypanosoma cruzi kDNA Minicircle Sequences into the Rabbit Genome.

To continue the investigation of host-pathogen interactions in the rabbit, four sexually mature does and two bucks were crossbred during chronic infection. After three pregnancies, the does with chronic *T. cruzi* infections delivered 104 litters (26 ± 6 per doe). Three controls, uninfected does in three pregnancies delivered 96 litters (32 ± 3 per doe). PCR was carried out on DNA from specific tissue of still born animals for both *T. cruzi* nDNA and kDNA (Figure 5 A and B).

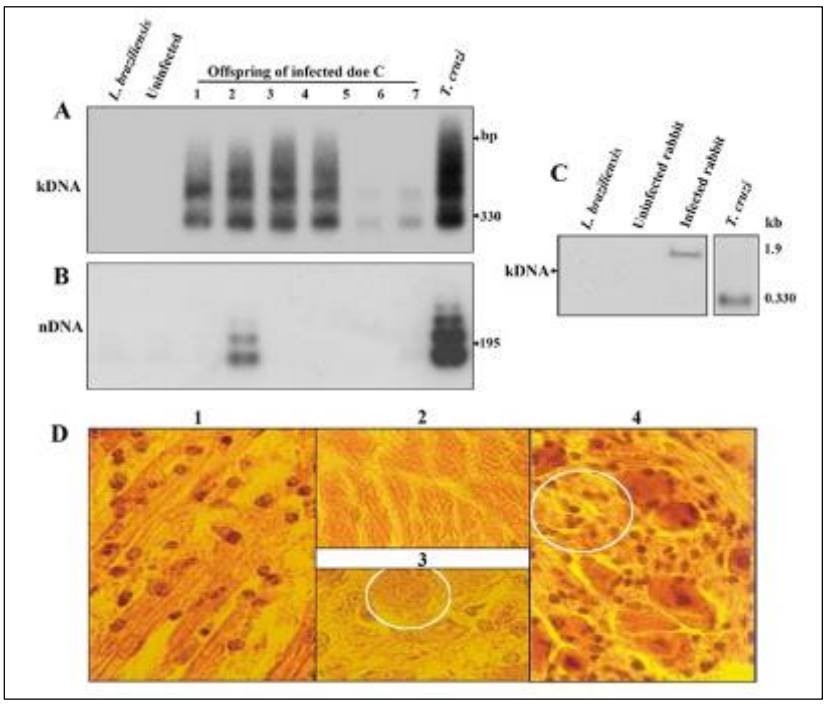

Figure 5 Genetic markers of *Trypanosoma cruzi* infection in offspring of Chagas disease rabbits, kDNA transfer, and pathology

Hybridization of PCR amplification products from template DNA obtained from offspring of Chagas disease Doe C, using sets of *T. cruzi* nDNA and kDNA primers, and specific radio labeled nCR and kCR probe.

Panel A) Evidence of genetic markers of the *T. cruzi* kDNA transfer. Specific hybridization of PCR amplification products from template DNA obtained from offspring of Chagas disease doe C using set of *T. cruzi* kDNA specific primers. The *Eco*RI digested DNA products resolved in 1% agarose gels. PCR analysis of kDNA amplification showed bands of 300 bp and its catamers from the parasite DNA and from genomic DNA of six progeny with hybridization with the kCR probe.

Panel B). PCR analysis of nDNA amplification shows bands of 188 bp and its catamers formed with parasite DNA and from genomic DNA of offspring 2 after hybridization with the specific internal probe. This event suggested vertical transmission of the *T. cruzi* infection from Chagas rabbits' parental to the offspring 2 of Doe C.

Panel C). Southern hybridization showing integration of kDNA minicircles into the genome of offspring from a *T. cruzi*-infected doe. Test and control DNA (20 *u*g) was digested with *Eco*RI along with 10 ng of *T. cruzi* or *L. brasiliensis.* DNA for Southern hybridization against the kCR probe. Separation of DNA products achieved as described in Figure 2. The presence of the 1.9 kb band size higher than the minicircle 330 bp band indicated the integration of the kDNA into the rabbit genome.

Panel D). Representative myocarditis and lysis of target cells from kDNA positive kitten 1 of Doe C. D1) Histopathological section showing mononuclear cell infiltration and lysis of target heart cells. Note the round lymphocytes adhered to the surface of the target cells and lysis. D2 and D3) Normal histological features of myocardium and of an intracardiac ganglion cells (white circle) from a control, noninfected kitten. D4) Intracardiac parasympathetic ganglion from a kDNA positive kitten showing mononuclear cell infiltration and neuron drop out (circle).

A sample showing the presence of kDNA but not nDNA (offspring 1 of doe C) was examined by Southern hybridization of *Eco*RI-digested genomic DNA with a kDNA probe. A band that was larger in size than the unit minicircle was detected, indicative of an integration event (Figure 5C). Southern hybridization of template DNAs from sperm and from unfertilized eggs from experimentally infected rabbits retained the kDNA 330 bp bands in the genome. The control uninfected rabbit DNA showed the absence of bands that hybridized with nDNA or kDNA probes. Out of the 104-surviving offspring from chronically infected parents, 24 (23%) contained kDNA as determined by the PCR assay. Nine stillborn yielded DNA from heart, skeletal muscle, liver, spleen, and large and small intestine, and each tissue type formed specific bands by hybridizing amplification products with a kCR probe. Figure 5D 1 and 4 shows myocarditis and ganglionitis in samples sections from kitten 1 from infected doe C. The control rabbit heart and ganglion tissue showed normal histology (Figure 5D 2 and 3).

This set of experiments demonstrated the vertical kDNA transfer to the genome of six progeny of the Chagas-rabbit, whereas the transmission of the *T. cruzi* infection was documented in progeny 2 showing a positive nDNA band. Although the kitten 2 harbored the persistent infection, the progeny showing kDNA fragments in diverse tissue types suggested that some integrations occurred shortly after parasite invasion thus, resulting in the transfer of kDNA throughout the embryo germline cells. In addition, the results showed that *T. cruzi* infections in rabbits as well as in humans can be vertically transmitted from males and females to mates by intercourse [44].

These experiments showed de novo transfer of kDNA to the rabbit genome is identical to its analog recognized in humans. The persistent *T. cruzi* infection in the benznidazole-treated rabbits there was a concern about artifact parasite DNA contamination of tissues from an infected host. To eliminate possible artifact, we tested the kDNA integration into chicken's refractory to *T cruzi* infection.

3.2 Chicken Model System

3.2.1 Integration of kDNA Minicircle Sequences from Trypanosoma cruzi into the Chicken Genome and Chagas-like autoimmune disease

To confirm and investigate the kDNA minicircle sequence integration into vertebrate host's genome, we moved our studies into chickens, which are refractory to *T. cruzi* infection. The pathology documented in the tissues from kitten 1 of Doe C suggested that an early embryo *T. cruzi* infection could transfer the kDNA minicircle sequences in germline and somatic cells genome and, therefore, the *ex vivo* uptake and invasion of the chicken blastula stage embryo stem cells was first explored [74]. The kinetics of the *T. cruzi* infections in fertile chicken eggs inoculated with 100 *T. cruz*i trypomastigotes prior to the incubation at 37 ºC were documented. On the eighth days of incubation, the embryo stem cells with the dividing amastigotes were identified by a fluorescein-labeled anti *T. cruzi* antibody and X-Gal staining. Using this immunohistochemical approach, we confirmed amastigotes of *T. cruzi* in chicken embryo endoderm and mesoderm tissues at embryonic stages 4 and 8 days old [50] The *T. cruzi* amastigotes in the embryo stem cells that were

examined by electron microscopy showed a typical disc-shaped kDNA network and membrane wrapped around the nucleus containing DNA (Figure 6).

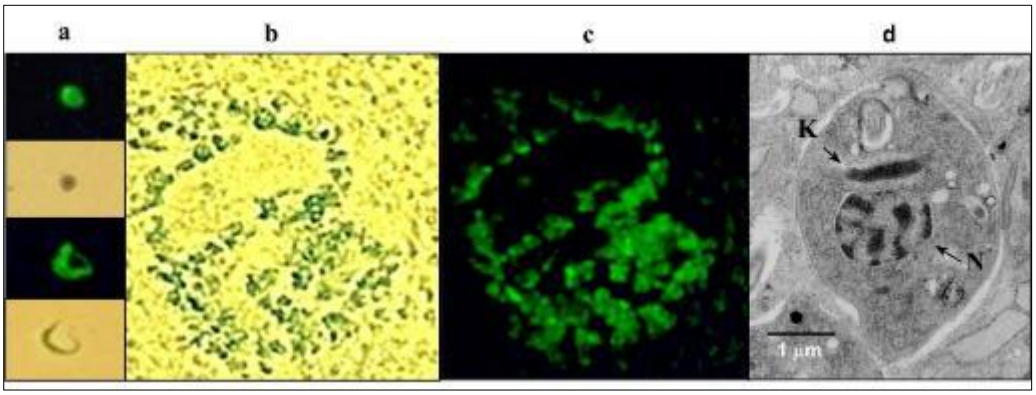

Figure 6 Growth of ß-galactosidase expressing *T. cruzi* in the avian embryonic stem cell

T. cruzi growth in endodermal and mesodermal cells of a 4-day-old chicken embryo. a) round amastigote and slender trypomastigote forms are stained fluorescent green because of recognition by a specific antibody from a patient with Chagas disease, and brown forms are the same unstained *T. cruzi* stages seen by phase contrast microscopy. (Magnification 1,200x). b) Paraffin embedded section showing blue X-Gal-stained cells in the endoderm and mesoderm tissues of a 4-day-old embryo. (Magnification 200x). c) Fluorescein-conjugated antibody-stained *T. cruzi*-infected cells colocalized in the same embryo tissue section. d) Electron micrograph showing an intracellular amastigote: k, kinetoplast; n, nucleus.

The permissiveness of embryonic stem cells to a *T. cruzi* infection of a 2-day-old zygote at the blastula stage was an indication of differentiating germline cells in the genital crest, which appear at days 4-8.5 of gestation [50]. Thus, germ line cells could encroach parasite-host cell interactions, displaying early drug inhibitor effect on cell growth, and prevention of kDNA transfer. In control experiments, we inoculated naked minicircle or cloned minicircle sequences in the air chamber of 30 fertile chicken eggs. Absence of PCR amplification products from these embryo's template DNAs tested weekly prior to hatching indicated that, as in rabbits, transfer of minicircle kDNA sequences to a bird's genome requires a living infection.

The experiments in the chicken model system were focused on the dissociation of kDNA integration from cryptic *T. cruzi* infection. Therefore, a kDNA integration event occurring early in the embryonic developmental process could result in the generation of a sexually mature chicken with kDNA integrated into gonadal tissue.

Thirty-six fertile chicken eggs were each injected with 100 *T. cruzi* trypomastigotes. The embryo tissue collected on the second, fourth-, and eighth-days post infection yielded nDNA and kDNA amplification products; however, tissue collected on the tenth, 12^{th}, 18^{th} and 20^{th} days of incubation yielded amplification products only for kDNA, indicative of the clearance of the active infection (Figure 7 A). The sensitivity of the PCR assay precluded the possibility of very low levels of parasitism in chicks hatched from *T. cruzi*-infected eggs, parentals, and offspring.

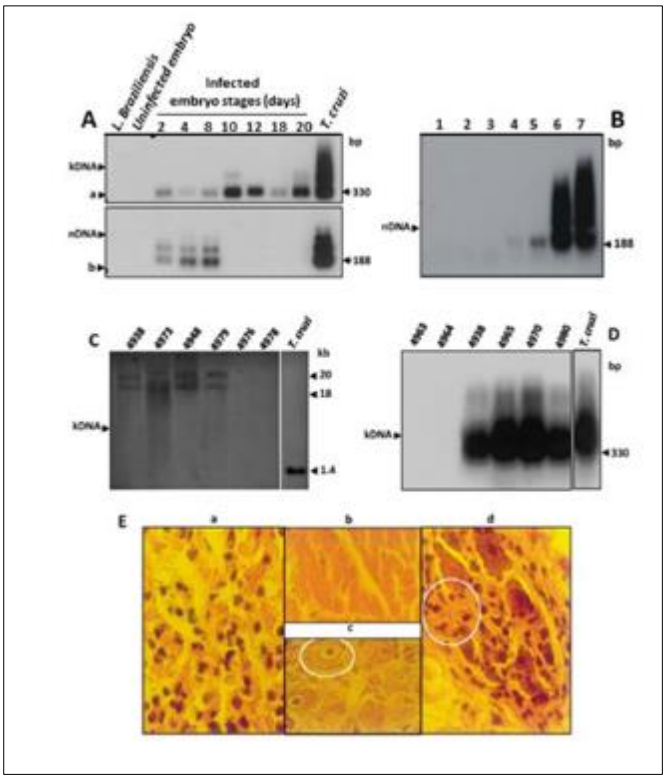

Figure 7 The kDNA integration in germ line cells and tissues from birds hatched from *T. cruzi*-infected eggs, with accompanying pathology**.**

kDNA integration in the embryo stem cells at blastula stage.

Panel A). Establishment of *T. cruzi* infection early in embryonic development followed by loss at 10 days of incubation. PCR, size separation, blotting, and hybridization were performed as described in Figure 2. Aa) Hybridization of PCR amplified bands of kDNA minicircles. kDNA products were amplified from DNAs harvested from tissues at several stages in the embryonic development of the chicken as indicated. Ab) Hybridization of PCR amplification of sequences of nDNA. Bands of 188-bp were diagnostic of nDNA presence in the template DNA.

Panel B). Sensitivity of the PCR amplification with nDNA primers Tcz1/Tcz2. The PCR products separated in 0.7% agarose gels, blot, and hybridization with the specific radiolabeled nCR probe, as described in Figure 2. Lanes 1 and 2, from kDNA-mutated and from control kDNA negative chickens. Lanes 3 to 7, mix of 200 ng of control chicken DNA with increasing amounts of *T. cruzi* DNA: 1 fg, 10 fg, 1 pg, and 100 pg, and 1 ng, respectively. The hybridization with the radio nDNA (nCR) probe detected 10 fg of the parasite DNA, which is 24-fold below the diploid *T. cruzi* nDNA.

Panel C). Southern hybridization of *Eco*RI digests of genomic DNA derived from *T. cruzi*-infected or uninfected eggs with a kDNA specific probe. Band sizes of approximately 20 and 18 kb formed with DNA from *T. cruzi*-infected birds 4938, 4973, 4948, and 4979 but not with DNA from uninfected, control birds 4976 and 4978. The positive control consisted of 10 ng of *T. cruzi* DNA.

Panel D). Integration of kDNA fragment into the avian germline. PCR hybridization analysis of template DNAs from sperm (4938 and 4965) and from nonfertilized eggs (4970 and 4980) from experimentally infected birds, compared to control birds 4963 and 4964. Probe and controls used are described in Panel A.

Panel E). Destructive myocarditis and ganglionitis in 2-week-old F1 chick 1072. Ea) Histopathological section showing mononuclear cell infiltration and lysis of target heart cells, like that described in Figure 5 D1. Eb) Normal histological features of myocardium. Ec) Normal histology of intracardiac ganglion neurons (white circle) from a control offspring of a noninfected chick. Ed) Section from an intracardiac parasympathetic ganglion showing lymphocyte infiltration and drop out of neuronal cells (circle). Consistently, niches of parasitic amastigotes were not present in the tissues from chickens hatched from *T. cruzi*-infected eggs.

To confirm the refractoriness of chickens to *T. cruzi* infections, we employed a PCR assay with the Tcz1/Tcz2 primers and hybridization of amplicons with the radiolabeled 188-bp nDNA probe. These experiments revealed that the sensitivity of the PCR assay (10 fg) was many-fold below the level of a diploid parasite (240 fg) nDNA and, therefore, the eradication of *T. cruzi* infections from the chicken body was no longer an issue (Figure 7B). These results validate the findings of kDNA minicircle sequence integration into germline and somatic cells. Furthermore, the presence of kDNA with mobility differential from naïve minicircles in the gonadal DNA of individual chickens combined with the absence of *T. cruzi* nDNA attested to the success of the integration event and of the subsequent eradication of *T. cruzi*.

Two roosters (4938 and 4973) and two hens (4948 and 4979) that hatched from *T. cruzi*-infected eggs, then showed positive hybridization bands with the kCR in a Southern blot performed on DNA isolated from sperm and from unfertilized eggs, with their pattern of migration differing from that of free-relaxed or of free-catenated minicircle DNA (Figure 7C). These birds were raised for crossbreeding. In the control group, 14 fertile chicken eggs were subjected to PCR, and neither nDNA nor kDNA was detected. Additionally, we inoculated naked minicircle or cloned minicircle sequences in the air chamber of 30 fertile chicken eggs. The absence of PCR amplification products from these embryo's template DNAs tested weekly prior to hatching indicated that, as in rabbits, transfer of minicircle kDNA sequences to a bird's genome required an early live *T. cruzi* infection.

To determine whether kDNA-transfected birds harbored *T. cruzi*-specific DNA in germline cells, we collected sperm from 4938 and 4965, and eggs at an early stage of development from the ovaries of hens 4970 and 4980. DNA templates that were extracted from these samples yielded kDNA but not nDNA amplification (Figure 7D). DNA from testes and ovaries of control, uninfected birds 4963 and 4964 did not yield products.

Histopathological lesions in muscle tissues and in peripheral nervous systems were seen in offspring that hatched from *T. cruzi*-infected eggs. Myocarditis and ganglionitis were visible, like those lesions described in the rabbit offspring (Figure 7E, a, and d). These diagnostic lesions were absent in tissues of control offspring from chicks hatched from uninfected eggs (Figure 7E, b, and c). In this respect, the inflammatory autoimmune rejection of parasite-free target host cells observed in birds with kDNA integration is like that seen in *T. cruzi*-infected rabbits and in humans with Chagas disease.

3.2.2 Germline Transmission of Integrated kDNA in Gallus gallus.

We examined the transmission of integrated kDNA to the resulting progeny chicken independent of persistent or cryptic *T. cruzi* infection. The kDNA-transfected rooster 4938 and hens 4973 and 4948 were bred to produce vertical, germline transmission of kDNA to their offspring (Figure 8A).

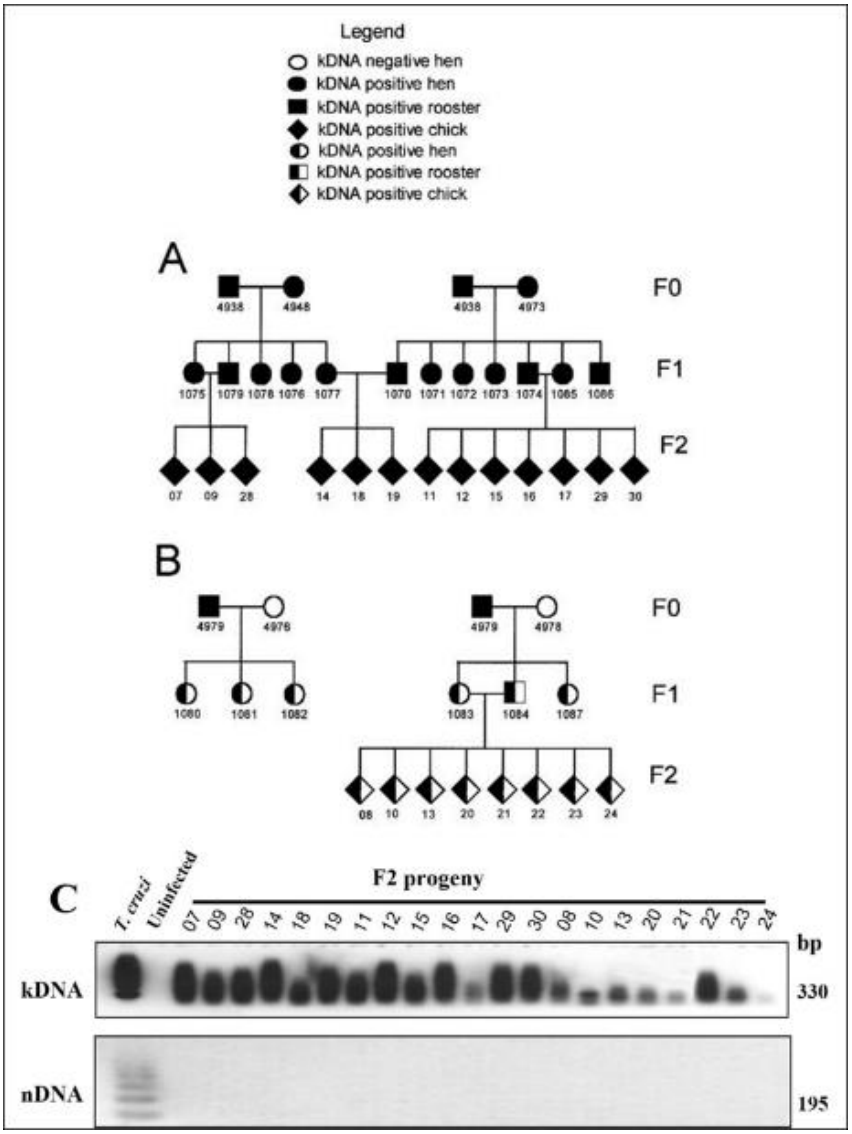

Figure 8 Pedigree of chickens carrying integrated kDNA

Panel A). Parentals kDNA-positive rooster 4938 kDNA-negative hen 4948 (FO) were crossed yielding five offspring each carrying the kDNA genotype. Similarly, kDNA positive rooster 4938 was crossed with kDNA-positive hen 4973, yielding seven offspring (F1) each carrying the kDNA genotype. Further crossing of F1 resulted in offspring, each carrying homozygous kDNA genotype (F2).

Panel B). Parentals kDNA-positive rooster 4979 was crossed with kDNA-negative hen 4976 (FO), yielding three offspring each carrying the kDNA genotype. Similarly, kDNA positive rooster 4979 was crossed with kDNA negative hen 4978, yielding three offspring carrying the kDNA genotype (F1). Further crossings of F1 positive rooster with negative hen resulted in offspring carrying hemizygous kDNA genotype (F2).

Panel C). Evidence of persisting kDNA but not nDNA in tissues from progeny of birds hatched from *T. cruzi*-infected eggs. The PCR hybridization assay performed as described in Figure 1A. a) Hybridization of PCR amplification of kDNA minicircles utilizing the kDNA primer set shows band size 330 bp and its catamers in each F2 progeny, which were not formed in uninfected, control DNA. Controls consisted of 10 ng of *T. cruzi* DNA and 20 *ug* of uninfected chick DNA. b) Absence of *T. cruzi* nDNA in progeny of germline kDNA parents. The 188-bp band and its catamers formed with the *T. cruzi* DNA only.

Twelve chicks born from these crosses carried kDNA in their genomes, as shown by amplification from blood cell DNA. The kDNA-positive F1 birds then crossed to obtain F2 hybrids, producing lineages of kDNA transfected progeny. KDNA transfected rooster 4979, and control, uninfected hens 4976 and 4978 were bred to detect the frequency of vertical

inheritance of kDNA to F1 and F2 offspring from a single kDNA donor parent. All chicks born from these crosses showed kDNA in their genomes thus, indicating that integrated kDNA can be inherited through the male (Figure 8B). Cloning and sequencing revealed kDNA (GenBank 531591 to 531759, S3 Table) integrated into the chicken genome. In a control PCR for nDNA, no bands were obtained from any of the offspring DNA samples (Figure 8C). These results validated the phenomenon of vertical transfer of *T. cruzi* kDNA into the chicken genome.

The mapping of the kDNA minicircle sequence integrations into the genome of 35 chickens hatched from the *T. cruzi*-inoculated eggs was performed (S3 Tables A and B). The databank analysis revealed kDNA integration with shearing of the transfers to large chromosomes into the chicken genome. These findings are explained by kDNA integrations into specific *loci* in the chicken genome through intraegg *T. cruzi* infection or through vertical transfer inheritance.

The *tp*Tail-PCR amplification products, cloning and sequence analyses revealed that transposable elements hitchhiked the mitochondrion kDNA-minicircle sequences into the gene encoding a cell surface glycoprotein derived neurotrophic receptor (FN 598 975) at chromosome 13, and into the alpha 3 gene encoding a glycosylphosphatidylinositol cell surface receptor signaling complex with tyrosine kinase receptor binding the ligand artemin at chromosome 2. In addition, samples of the kDNA mutations (FN 598 972 and FN 598982) into coding regions of serine/threonine protein kinases and phosphatases, playing roles in signaling and adaptation to environments, were found at the chromosome 14. Furthermore, the kDNA mutations (HG531472) inserted at the Dystrophin gene, encoding an associated protein complex scaffold various signaling proteins, at chromosome 1. The GenBank data with further kDNA mutations, showing gene reshuffling and remodeling at several chromosomes are displayed at S3 Tables A and B.

In this study, the separation of the kDNA minicircle sequence integration event from active infection with *T. cruzi* unequivocally indicates that our observations are valid. With this respect, the functional consequences of kDNA integration sequence were sought at bone marrow cells progenitors of effector cells, causing an autoimmune reaction against heart tissue antigens. However, the protein extracts from kDNA+ and kDNA- chicken heart showed identical protein profiles in three independent two-dimensional gel electrophoresis (2DE). The immunoblotting experiments confirmed identical profiles.

3.2.3 Chagas-Like Clinical and Pathological Manifestations in Chickens

The kDNA-mutated chickens developed clinical symptoms like those of rabbit and of human Chagas disease. The kDNA+ and the healthy kDNA- chickens were inspected weekly. Signs of shortness of breath were observed in the kDNA+ chickens, and cyanosis (Figure 9A), ascites, and pleural effusions were constant ominous signals of heart failure in the kDNA-mutated group of chickens. The ECGs recorded at three and at six months in 12 F0 kDNA-mutated chickens and in 22 kDNA-negative controls, showed the test birds changed the axis position to the left from +80 to – 115º over time, whereas the controls retained the electric axis at + 75º. Ascites and pleural effusions were collected in kDNA-mutated birds with heart failure (Figure 9B).

The parasite free-pathology-translated clinical findings in a chicken hatched from the *T. cruzi*-infected egg, showing kDNA mutations in chromosomes 2 and 13.

Panel A). Nine-month-old chicken with heart insufficiency and cyanosis (left), and a control hen of the same age showing a bright red comb (right). B) ECG alteration with shift of cardiac axis from a-to-c over a six-month period. C) The body heart weight indexes showed statistically significant differences ($p<0.05$) in control and in kDNA-mutated chickens. D) Cardiomegaly (30 g) in a nine-month-old hen that died of heart failure. E) Control heart (15g) from a nine-month-old hen. F) Diffuse myocarditis showing cytotoxic lymphocytes infiltrates and lysis of target heart cells. The red cycles depict minimum rejection units where several lymphocytes lysis a target cell. G) Normal myocardium histology of an adult hen. H) kDNA-mutated chicken, intracardiac parasympathetic ganglion showing mononuclear cell infiltrates and neuronal cell lysis; I) Control, normal histology of an intracardiac ganglion. J) Lack of B cell after treatment with anti-Bu-1 monoclonal antibody. K) CD45+ lymphocytes identified (arrows) in heart lesions by a phycoerythrin-labeled specific monoclonal antibody. L) CD8+ɣð immune lymphocytes (arrows) involved in severe destruction of the heart. M) Abundant CD*α+ T cells in severe lesions with heart cell lysis. N) Monocytes and macrophages in the heart lesions.

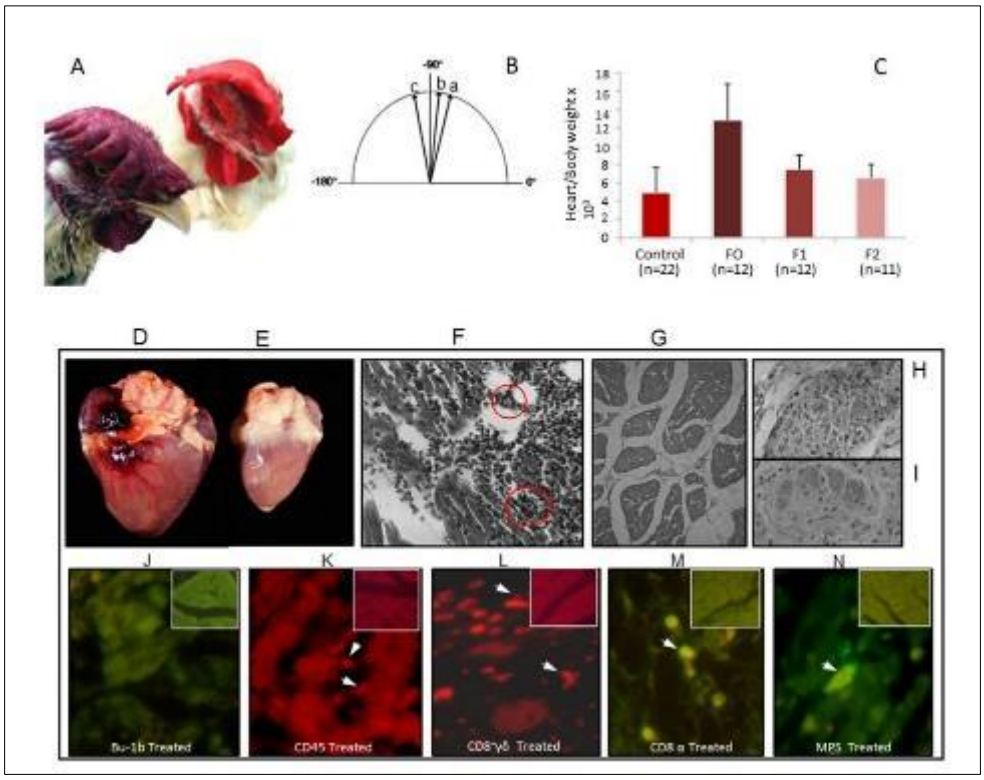

Figure 9 Clinical and pathological findings in *Gallus gallus* with kDNA-integrated minicircle sequences into the genome

The kDNA-mutated chickens heart body weight indexes ranged from 6 ± 2; to 6.7 ± 2, and to 12 ± 5. In the control chicken group, the index was constant at 4.2 ± 2. We documented statistically significant differences among the high heart size indexes from F0 and from F1 kDNA-mutated chickens from those low indexes from controls ($p<0.05$). Consistently, survival length for those groups of kDNA-mutated chickens were shorter for F0 (12±4 months) and F1 (13±2 months) than those in the control group (19 ±5 months). These differences are statistically significant ($p<0.05$) (Figure 9 C).

The gross pathology in birds hatched from *T. cruzi*-infected eggs consisted of cardiomegaly like that seen in human Chagas disease. The chickens' hearts showed thickening of the walls of the ventricles and dilation of the chambers (Figure 9D**)**. Control, healthy chickens showed normal heart size (Figure 9E). In these experiments, the histopathological analysis of the myocardium showed destruction of parasite-free heart cells by effector mononuclear cells and depicted the hallmark rejection of the target cell (Figure 9F), characterizing minimal rejection units (red circles) in the myocardium. The control sections of the myocardium showed normal histology (Figure 9G). The finding of the parasite in the heart was unexpected because the chicken's innate immunity eradicates *T. cruzi* infection. Ganglionitis with lysis of target cells were observed in the Figure 9H), but these features were not observed in the control parasympathetic neurons (Figure 9I). Those inflammatory infiltrates reached the wall of the intestines and skeletal muscles. The antibody producing B-lymphocyte was not present in those inflammatory infiltrates (Figure 9J). However, the immunohistochemical assays of myocardium from kDNA-mutated chickens treated with anti-CD45, anti-CD8γδ, or with CD8α and macrophages treated with MPS antibody (Figure 9, K to N) showed specific staining of these lymphocytes carrying out lysis of target heart cells. In control experiments, section from myocardium of control chickens (inserts) showed neither markers of any cytotoxic lymphocytes nor tissue destruction.

Chickens with mutations in the dystrophin gene showed myocarditis with inflammatory cell infiltrates in the heart and skeletal muscles showing severe lysis (Figure 10 A and B). Additionally, the parasympathetic nervous system showed lymphocyte infiltrates and neuronal cells lysis (Figure 10, A-to-E).

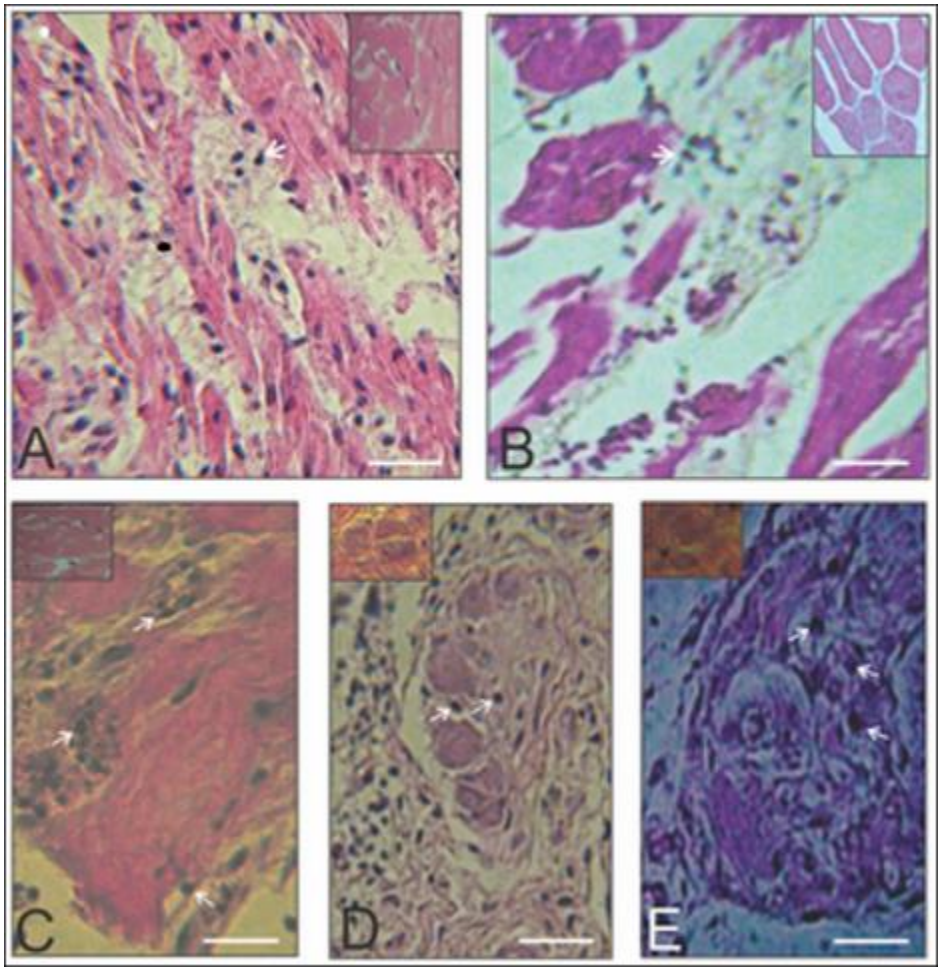

Figure 10 Pathology in the heart, parasympathetic ganglia, and skeletal muscle of a dystrophin gene kDNA-mutated rooster

Myocarditis, myositis and ganglionitis in a rooster with a kDNA minicircle sequence mutation (RG531472) in the dystrophin gene.

Panels A and B). Heart (left) and skeletal muscle (right) showing lysis of target cells by cytotoxic lymphocytes (arrows). Inserts show normal tissues histology.

Panel C). Myositis with lysis of the striated muscle cells by lymphocytes (arrows).

Panels D and E). Parasympathetic ganglia of the large bowel (middle) and of the heart (right) showing inflammatory infiltrates (arrows) and neuron lysis. Hematoxylin-Eosin-stained sections. Bars, 10 μm.

These findings show that insertions of kDNA minicircle sequences in transposable elements could hitchhike to several coding regions in the chicken genome, thus, to initiate autoimmune rejection of body tissues over time. The control chickens showed normal histology (inserts).

In view of these results, we investigated whether the multidrug treatment of *T. cruzi* infection with the lead compound benznidazole in combination with drug inhibitors could prevent eukaryote cell division and growth *ex vivo* and inhibit the kDNA transfer.

3.2.4 Searching for Drug Inhibitors of T. cruzi kDNA Transfer

The selected array of inhibitors of eukaryote cell growth was aimed at the multidrug treatment of *T. cruzi* infections with specific objectives: *i*) lethal effect against the *T. cruzi* forms; *ii*) minimal toxicity to the host cell; *iii*) abolishment of kDNA transfer. The metabolic pathway inhibitors optimal concentration determined by the *in vitro* dose response.

The better inhibitors were selected in triplicates ex-vivo experiments using different drug concentrations. The optimal dose was determined for *T. cruzi* epimastigote (10 x 10^6/mL) incubated for 4 h at 27 ºC with each drug at a concentration, two times above, and two times below the optimal dose (Table 4). After that incubation period, the cells were transferred to culture tubes containing agar slants with LIT medium overlay. Three repeat experiments were conducted to determine the drug concentration killing effect in aliquots of specific inhibitor-treated *T. cruzi* forms suspended in fresh LIT medium and growth in a shaker incubator at 27 ºC for 8 days. The motile epimastigotes showing typical whitish silhouettes in a counting chamber, which were recorded and plotted, and the cytotoxic effect of each inhibitor shown in Figure 11 A to D. The drug concentration that killed 75% and above the *T. cruzi* epimastigotes in LIT medium during a one week were chosen.

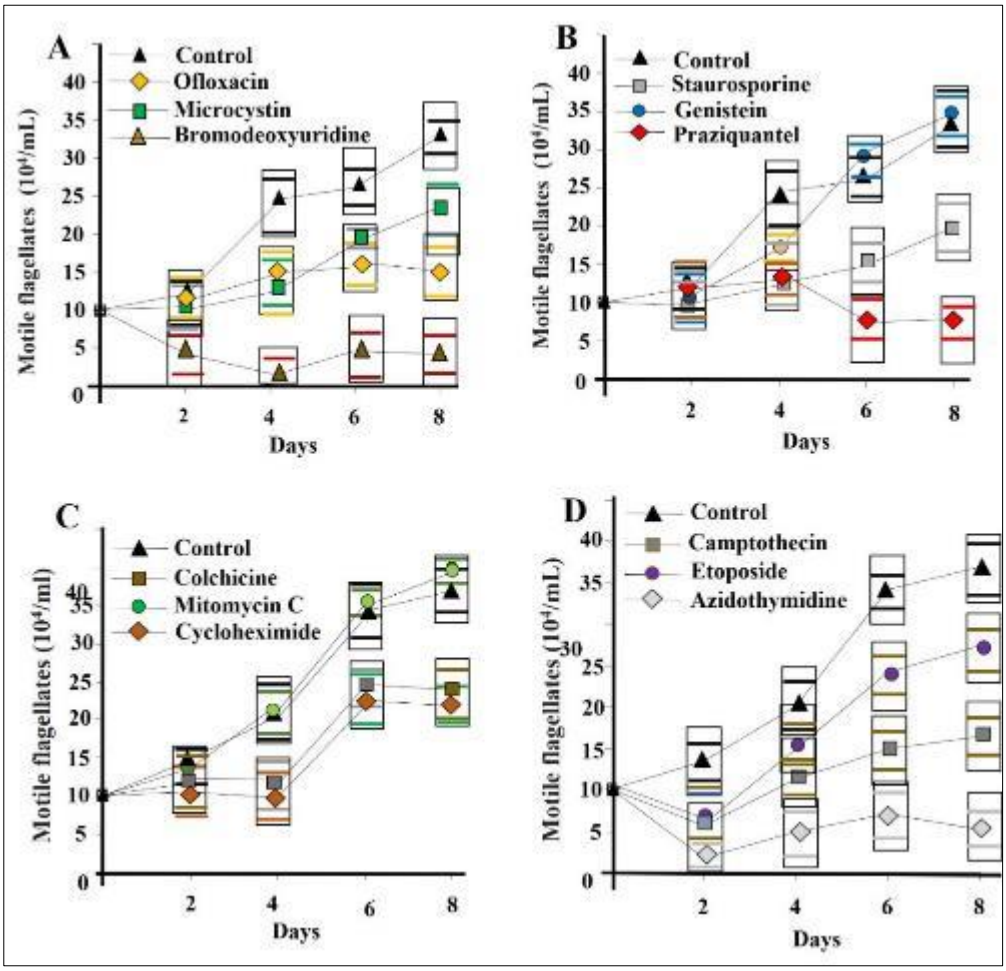

Figure 11 The effect of specific inhibitors of cell growth and differentiation on the *Trypanosoma cruzi* epimastigote form

The cytopathic effect recorded at two-week incubation, staining and microscopy from three independent experiments.

Panels A, B, C and D). Lethal effect of inhibitors of *T. cruzi* epimastigotes. The findings revealed that bromodeoxyuridine, azidothymidine, praziquantel, and ofloxacin, respectively, killed 96%, 94%, 92%, and 85% of the epimastigotes. Growth curves depicted the white, motile parasites. The parasite killing was confirmed in trypan-blue dye staining of immobile flagellates. Note that ofloxacin (A), praziquantel (B), and AZT (D) showed high lethal effect upon the flagellates. The remaining of the drugs showed much less pathogen killing activity. The inhibitor concentration showing lethal effect upon *T. cruzi* epimastigotes and undetectable toxicity to the muscle cells was employed in the *ex vivo* investigation.

The experiments further assessed the drug inhibitor toxicity against the L6 muscle cells. A suspension of 10 x 10^5/mL muscle cells in DMEM was incubated with the optimal inhibitor concentration shown in Table 4. Three independent repeat experiments were performed for each of twelve drug inhibitors. The mock control *T. cruzi*-infected muscle cell suspension was maintained in the absence of the drug inhibitors. After 14 days incubation the muscle cell monolayers were washed with PBS, stained with H-E, and examined. The moderate and severe toxicity of the inhibitors on the target

cells revealed the blurred fade-away silhouette of some amastigotes, whereas the muscle cells showed loss of membrane boundaries and cytoplasm vacuolation. None of these features were seen in the cells in the absence of a drug inhibitor. These experiments revealed severe toxicity of microcystin, bromodeoxyuridine, and mitomycin on muscle cells. Cycloheximide, staurosporine, genistein, etoposide and camptothecin showed moderate toxicity, and praziquantel showed mild toxicity. Ofloxacin and Azidothymidine that killed the *T. cruzi* epimastigotes did not kill the L6 muscle cells and, therefore, they were selected for *in vivo* experiments in the mice models.

3.2.5 T. cruzi-Macrophage Cocultures and Assessment of the Infected Cells DNA.

The parasite persistence within a mammalian is hidden from the host immune system inside nonphagocytic cells [75, 76]. Because the integration of *T. cruzi* minicircle kDNA sequences into the macrophage genome would cause host cell-pathogen interactions this phenomenon was investigated *ex-vivo*.

Having identified the dose of each inhibitor that did not kill muscle cells, we investigated the effect of the drug-mediated inhibition of kDNA transfer to the genome of *T. cruzi*-infected human macrophages. The Southern blot analysis of the *T. cruzi*-infected macrophage DNA-PCR amplification products obtained with specific primer sets and radio labeled kCR probe showed that the phosphorylases, polymerase II, and late phase cell division inhibitors: mitomycin, cycloheximide, etoposide, genistein, ofloxacin, praziquantel, and staurosporine, prevented the formation of the large 1.2, 1.8, and 2.2 kb kDNA minicircle sequence bands. In addition, colchicine, which suppress tubulin assembly and microtubule formation, and azidothymidine, which intercalates thymidine to DNA, inhibiting reverse transcriptase and telomerase at the G2/M cell growth phase, abrogated the transfer of large 1.2, 1.8 and 2.2 kb kDNA sequence bands (Figure 12).

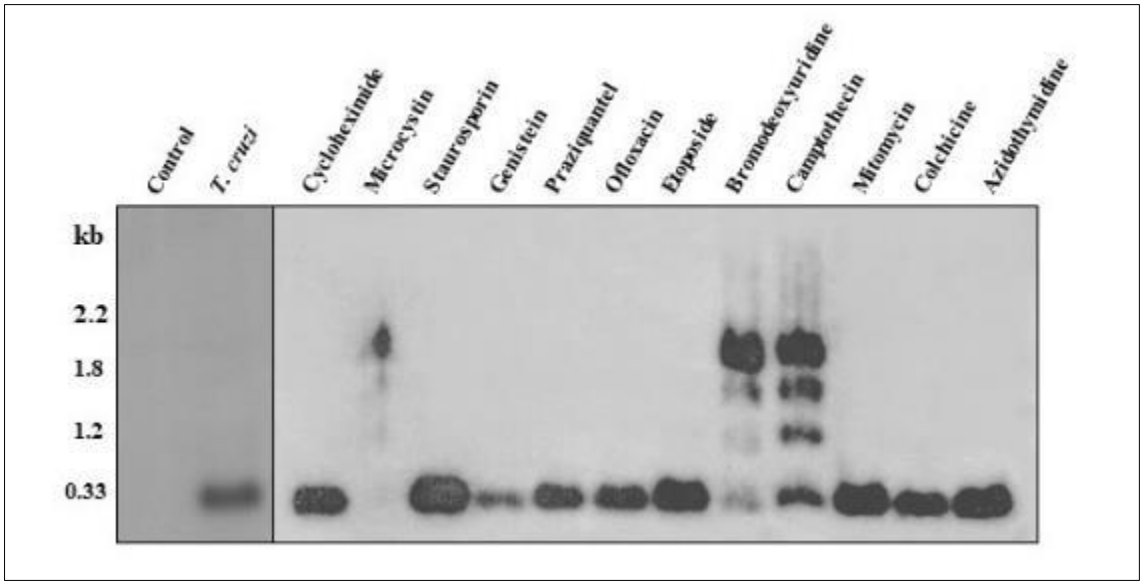

Figure 12 *Trypanosoma cruzi*-macrophage cocultures and assessment of the DNA at day-21st post treatment with inhibitors of cell growth and development

The PCR amplification products were separated in a 0.7% agarose gel, blotted, and probed with the radiolabeled kCR probe for the conserved minicircle sequence. The results are representative of three repeat experiments. Note that the microcystin concentration that killed *T. cruzi* and prevented 0.330 kb band formation did not inhibit the integration of the kDNA band forming the upper 2.2 kb band, whereas bromodeoxyuridine and campthothecin did not abrogate kDNA bands. The other inhibitors prevented large 1.2, 1.8, and 2.2 kDNA bands but they did not inhibit the 0.330 kb band formation. The positive control *T. cruzi* kDNA formed a typical 0.330 kDNA band, and the control DNA showed no band.

In contrast, microcystin, camptothecin, and bromodeoxyuridine, respectively, inhibitors of phosphatases and polymerase I, that form DNA adducts at phase S cell cycle, did not inhibit the transfer of the 1.2, 1.8 and 2.2 kb bands into the host cell. Interestingly, microcystin, a serine/threonine phosphatase PP1 and PP2A inhibitor, inhibited the formation of the 0.330 kb kDNA band only. The PCR amplification of the purified *T. cruzi* kDNA showed a single 330 bp band only, whereas the *T. cruzi*-infected macrophage DNA yielded the 330 bp band, and, in addition, it formed 1.2, l.8, and 2. 2 kb kDNA bands. The control macrophage DNA showed no band (Figure 12).

The macrophages were collected at day 21 post-infection with *T. cruzi* and treated with the inhibitor concentration. The DNA-PCR amplification products hybridized with the radio labeled kCR minicircle probe revealed that phosphorylases, polymerases, and late phase cell division inhibitors precluded the transfer of the 1.2, 1.8, and 2.2 kb kDNA bands into the macrophage genome. Microcystin, campthotecin, and bromodeoxyuridine did not prevent the transfer of the sequences detected at high molecular-weight bands. Microcystin prevented the formation of 0.330 kb kDNA band.

The modification of band profiles indicated that kDNA minicircle sequences transfer into the host cell genome represent a persistent element in host-pathogen interactions. The persistence of the kDNA upper band sequences in the macrophage genome was observed over several years, and the cells were maintained in tissue culture. In this respect, we searched for drug inhibitors of the phenomenon of *T. cruzi* kDNA transfer into the host cell genome.

3.3 Mouse Models

3.3.1 Multidrug Treatment of T. cruzi-Infections

To confirm and dissect the effect of the drug inhibitors on eukaryote cells growth, we moved our studies into the mouse model system, which shows short lifespan and is sensitive to *T. cruzi* infection [77]

The evidence of kDNA integration into the macrophage genome led us to anticipate a therapeutic regimen encompassing the combination of drug inhibitors (Table 4) with the lead benznidazole for the treatment of Chagas disease. On the one hand, we used the azidothymidine that intercalates thymidine to inhibit reverse transcription, and apoptosis. On the other hand, ofloxacin 4-Fluorquinolone inhibits the polymerases metabolic pathway at G2/M phase, and apoptosis. In addition, the praziquantel quinolone derivative enantiomer was administered to *T. cruzi*-infected mice. This experiment aimed to determine whether the multidrug treatment that curtailed the infection would prevent the lateral transfer of kDNA integration into the mouse genome and associated pathology. Groups of eight mice each were inoculated with the *T. cruzi* trypomastigotes (2 x 10^3) intraperitoneal, and multidrug treatment regime by gavage initiated at the 5th day post infection; the *T. cruzi*-infected-untreated was the positive control group.

The results of these experiments showed that independent administration of either benznidazole, azidothymidine, ofloxacin, or praziquantel to treat each of eight acutely *T. cruzi*-infected BALB/c mice curtailed the presence of the protozoan flagellates in the blood from 40 to 20 days (Figure 13A).

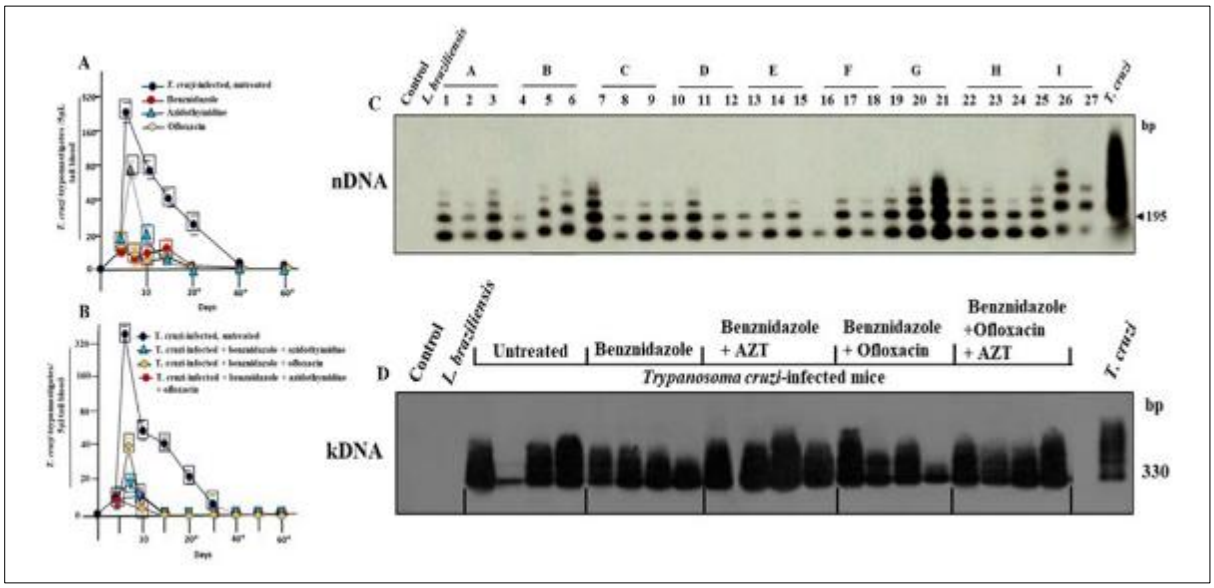

Figure 13 Profiles of parasitemia in *T. cruzi*-infected mice treated with benznidazole and drug inhibitors of eukaryotic cells growth

Panel A) The peak of parasitemia detected in *T. cruzi*-infected-untreated mice. A quick fall was observed in the *T. cruzi*-infected groups of mice treated with either benznidazole or azidothymidine, or ofloxacin clearing tail blood (5*u*L) parasitemia at day 20.

Panel B) Curtailment of parasitemia. The parasitemia undetectable at the 40th day in the untreated group of mice, whereas it lasted for 15 days in the *T. cruzi*-infected-mice treated with the combination of benznidazole-ofloxacin or with the benznidazole-azidothymidine. The results further showed the parasitemia abbreviate to 15 days in the group of mice treated with benznidazole, azidothymidine and ofloxacin. The asterisks under the abscissa indicated, however, that the hemocultures set at the 20th, at the 40th, and at the 60th days post infections yielded *T. cruzi* species.

Panel C). Southern hybridization of *T. cruzi* nDNA-PCR product from *Mus musculus* subjected to a therapeutic regime. All the DNA samples yielded 188 bp bands that confirmed *T. cruzi* infection. The blood of *T. cruzi*-infected mice group A as well as the groups B to H subjected to either benznidazole (group B) alone, or in combination with different inhibitors (groups C to H). The treatment did not eliminate the infection, since the *T. cruzi* nDNA band 188 bp was retained in mouse body.

Panel D. Southern hybridization of *T. cruzi* kDNA-PCR product form *Mus musculus* subjected to a multidrug therapeutic regime. The solid tissues from each group of mice (n = 8) were minced with sterile blades, and the tissue subjected to DNA extraction and purification. The PCR amplification products analyzed in agarose gel electrophoresis, blotting, and Southern hybridization with a radio labeled kCR probe. Note the 330 bp kDNA band in groups of *T. cruzi*-infected mice; *i*) untreated; *ii*) benznidazole-treated; *iii*) benznidazole, azidothymidine and ofloxacin treated. B, blank; C1 and C2, uninfected controls; *T. cruzi*, positive control

The evidence of toxicity prevented administration of praziquantel in other mouse groups. In addition, the experiments showed that further abolishment of the flagellates in the blood was achieved with the two-by-two combination of benznidazole with azidothymidine, and with benznidazole and ofloxacin: the employment of the lead nitro heterocyclic compound in combination with azidothymidine and ofloxacin, inducers of cell growth inhibition and apoptosis, curtailed parasitemia from 40 to 15 days (Figure 13 B). On the 250th day post infection, the mice of all groups were sacrificed under anesthesia, and the tissues were collected by necropsy. The body tissue samples were minced and processed for DNA purification and analysis. The persistence of the *T. cruzi* infections in the mice of each group was demonstrated further by PCR amplification with nDNA specific primer sets and with Southern blotting hybridization (Figure 13 C).

In view of the curtailment of parasitemia's and abrogation of the 330 bp kDNA band in the *ex vivo* macrophage assay, we run experiments to assess the effect of the multidrug treatment in preventing kDNA minicircle sequences integration into the mouse genome.

The ofloxacin and praziquantel piperazine derivative enantiomers inhibited *T. cruzi* growth *in vitro*. However, the mild cytotoxicity of praziquantel against murine muscle cell suggested its exclusion from therapeutic regimen given to the *T. cruzi*-infected mice. In this regard, we continued the experiments assessing the inhibition of the lateral transfer of the kDNA minicircle sequence to the Chagas disease mouse genome. The results of the *T. cruzi* kDNA PCR-amplification with the S35/S36 primers, separation of the products in a 0.8% agarose gel, blotting, and radio labeling with the radio labeled specific kCR probe. This qualitative PCR technique is direct evidence of the presence of some 330 bp kDNA minicircle sequences integrated into the genome of the *T. cruzi*-infected mice treated with the lead multidrug therapeutic regimen (Figure 13D).

In previous experiments, we showed kDNA minicircle sequence integration into the genomes of *T. cruzi*-infected rabbits, and in chickens hatched from the *T. cruzi*- inoculated eggs. The *tp*TAIL-PCR techniques with the specific primer sets revealed the main site of the kDNA minicircle sequence integration into the rabbit (LBNL-1) and chicken (CR-1) LINE-1 retrotransposons on several chromosomes. Moreover, we showed that 70.8% of the *T. cruzi* kDNA integrations were observed in retrotransposons LINE-1 into the human genome (EMBL HG008116 to HG008708, S4 Table). Figure 1 depicts the schematic representation of the qualitative *tp*TAIL-PCR employed to disclose the kDNA mutations in the *Mus musculus* genome. The primers specific to mouse LINEs families, and the annealing temperatures are shown in Tables 5 and 6. The procedure included the uninfected mouse DNA and *T. cruzi* DNA internal controls, and the last cycle of the *tp*TAIL-PCR showed the host-*T. cruzi* DNA chimeras, only. The A/C rich nucleotide microhomologies at the site of integration in the mouse DNA, and in the kDNA minicircle constant sequence repeats intermediated nonhomologous end-joining recombination and lateral transfer of the *T. cruzi* mitochondrial minicircle sequence. The quantitative nucleotides searches proceeded throughout the GenBank/EMBL/DDBJ and Refseqs database. The masker CENSOR was used, and the redundant sequences were excluded by alignment with those in the mouse LINEs families. (Table 7 and S5 Table).

Table 7 Transfer of the *Trypanosoma cruzi* kDNA minicircle sequences into the mouse genome

Class	Type	Repeat	Transfers
Retrotransposon non-LTR	LINE-1 A	L1_MM	50
	LINE-1 A	L1P_MA2	18
	LINE-1 A	Lx7_3end	3
	LINE-1 A	L1_Mur3_orf2	3
	LINE-1 T_F	Lx3B_3end	2
	LINE-1 G_F	L1B_MM	1
	LINE-1 F	L1Md_F_5end	1
LTR	Mouse putative LTR	RLTR27_MM	2
ERV	Intracisternal *A-type* particle (IAP)	IAPLTR4_I	2
	Mouse virus-like 30S LTR	RLTR6_MM	1
Not determined			11
Total			94

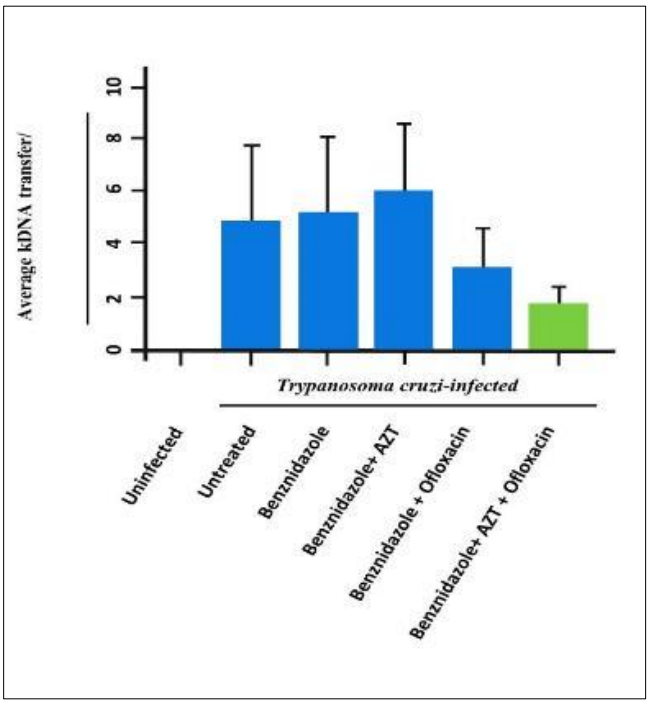

Figure 14 The inhibition of *Trypanosoma cruzi* kDNA minicircle sequence integration into the *Mus musculus* genome

In these experiments, mixed tissue DNA from each mouse was subjected to four independent repeat triplicate samplings of *tp*TAIL-PCR and the average nonredundant hybrid sequences, which were obtained from each of five experimental groups of mice, as shown in Figure 14.

Schematic representation of the average kDNA transfer in *T. cruzi*-infected groups of mice treated with lead compound benznidazole in combination with azidothymidine and ofloxacin. The average nonredundant kDNA transfer into each *T. cruzi*-infected mouse group (n=8) revealed the following: group I, untreated, 4.9 ± 2.6; group II, treated with benznidazole, 5.2 ± 2.7; group III, treated with benznidazole + azidothymidine, 6 ± 2.4; group IV, treated with

benznidazole + ofloxacin, 3.4 ± 0.9; group V, treated with benznidazole + azidothymidine + ofloxacin, 2.0 ± 0.4. This last group of kDNA mutations showed statistically significant differences ($p<0.05$) in the mice group I to III. This result is 2.44-fold below the total number of mutations in comparison to those disclosed in the genome of *T. cruzi*-infected, untreated mice.

In brief, a 2.44-fold inhibition of the lateral transfer of the *T. cruzi* kDNA sequence by the multidrug administration of the trypanocide benznidazole with azidothymidine and ofloxacin, which are inhibitors of host cell growth, was demonstrated.

The hybrid sequences with an average size of 505 ± 260 nucleotides are displayed in Table 7. The data revealed that 79% of the lateral transfers of the kDNA minicircle non-redundant sequences took place at Family A, LINE-1 into the genome of the *T. cruzi*-infected mice (S5 Table).

Moreover, the pathology study revealed that the control group of mice (Figure 15 A and B) showed normal heart size and histology.

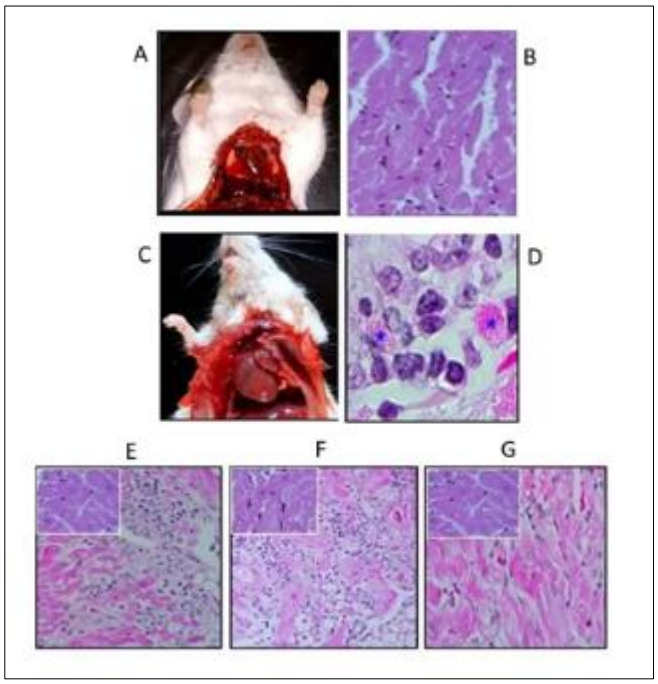

Figure 15 The quenching of the myocarditis in mice treated with benznidazole + azidothymidine + ofloxacin

Panels A to G). Quenched Chagas heart myocarditis. A) The uninfected, control adult mouse heart size. B) Normal heart histology of a control, uninfected mouse. C) Dilated cardiomyopathy of a benznidazole-treated Chagas' mouse. D) Inflammatory autoimmune rejection and the destructive myocarditis with lysis of the target heart cells (minimal rejection unit, asterisks) in a chronically *T. cruzi*-infected mouse, in the absence of amastigote nests *in situ*. E) Myocarditis of a mouse treated with benznidazole and azidothymidine. F) Similar myocarditis seen in a mouse treated with benznidazole and ofloxacin. F) Quenching myocarditis in a mouse treated with a cocktail of benznidazole, azidothymidine and ofloxacin. Notice that the representative histopathological findings in mouse group G was in keeping with lowered kDNA integrations into the genome.

Severe cardiomegalyy and intense heart cell lysis were present in the *T. cruzi*-infected- untreated mice myocarditis (Figure 15 C and D). Myocarditis and heart cell lysis were observed in the mice groups (Figure 15 E and F) treated with benznidazole combined with either ofloxacin or azidothymidine. Of interest, a reduced myocarditis and target heart cell lysis were documented in the group of rabbits that received benznidazole + ofloxacin + azidothymidine (Figure 15 G).

In conclusion, the histopathology showed that the benznidazole + azidothymidine + ofloxacin therapeutic regime prevented the myocarditis, and reduced the target cell lysis, which is a hallmark of autoimmune Chagas cardiomyopathy, in the absence of the parasite *in situ*.

4 Discussion

The scientific knowledge sheds light on the pathogenic mechanisms underlying the protean clinical manifestations underpinned by the transfer of *T. cruzi* kDNA minicircle sequences into the host's genome and the development of the hallmark cardiomyopathy of Chagas disease. The employment of cross kingdom animal models showed that the chicken's refractory to the *T. cruzi* infection retained the kDNA minicircle sequences integrations into the genome and developed the typical myocarditis of Chagas disease. The clinical-pathological manifestations of the disease, such as cyanosis, shortness of breath, pleural effusions and ascites, increased heart size and myocarditis were documented. The absence of *T. cruzi* nDNA in chickens hatched from eggs inoculated with the flagellates substantiates the cardiomegaly in the kDNA-positive chicken contrasted with the small heart size of the kDNA-negative control chicken. The myocarditis documented in the kDNA-positive chickens hatched from *T. cruzi*-infected eggs was identical to that of Chagas disease in humans, rabbits, and mice. The microscopic analysis of the myocardium revealed severe infiltrates of lymphocytes and target cell lysis. These microscopic features were absent in the heart of kDNA-negative, control chickens.

Several integrative review articles that describe the clinical-pathological manifestations of Chagas disease have suggested divergent pathogenesis mechanisms [23, 27, 78-82]. Those approaches put forward that *T. cruzi* and host genetic heterogeneity, whole parasite antigen, myosin autoantigen, molecular mimicry, cross-reactive antigens, anti-myosin antibodies, cytokine pattern changes, innate and acquired immune factors play roles in the physiopathology of the Chagas heart disease [25, 26, 78-83]. However, the pathology of Chagas disease has not been reproduced in a suitable animal model challenged with any of those factors, and molecular predictors of the myocardiopathy are none [26].

The Chagas-like cardiomyopathy is produced in the chicken model system that eliminate naturally the parasite and retain the kDNA minicircle sequence mutations in the genome. The kDNA-mutated chickens develop the Chagas-like cardiomyopathy indistinguishable from that seen in rabbits, mice, and humans. The direct evidence of kDNA minicircle sequence mutations and Chagas cardiomyopathy is documented in parasite-free chicken model showing rejection of self-heart cells by immune T-lymphocytes. The kDNA mutations in the hosts' genome, therefore, is a genuine biomarker to monitoring the efficacy of multidrug treatment of Chagas disease. [44, 50, 83, 84].

We reproduced the Chagas heart disease in the rabbit model infection system that developed Chagas disease indistinguishable from that described in humans [66, 67] The active process of genetic transfer between *T. cruzi* and rabbits was initiated with the examination of the effect of lead benznidazole in the treatment of Chagas disease [50, 67-71]. With this respect, a treatment strategy compatible with disease pathogenesis was hypothesized. For the lack of irreversible drug elimination of the *T. cruzi* infection, we sought to curtail the parasitic load, and to lower the accumulation of the kDNA minicircle sequences integrating into the host's genome, therefore, reducing polygenic modifications that could exacerbate the parasite-induced, genetically driven autoimmune mechanism lethal to approximately one third of the Chagas disease patients. The hypothesis addressed the autoimmune rejection of self-tissue inhibition by multidrug treatment of Chagas heart disease, and prevention of *T. cruzi* kDNA minicircle sequence integration into host cells genome.

We tested an array of drug inhibitors of eukaryote somatic and germ line cells metabolic pathway checkpoints. The optimal concentration of each of 12 drug inhibitors was tested *in vitro* against the *T. cruzi* forms. These experiments revealed the growth inhibitory efficacy of bromodeoxyuridine, azidothymidine, ofloxacin, and praziquantel in three independent replicate experiments. The trypan blue exclusion dye test showed that these inhibitors of eukaryote cells growth and differentiation killed over 75% of the flagellates after 8-days of incubation at 27 ºC. To determine the cytotoxicity of the array of 12 inhibitors, we incubated each drug with monolayers of *T. cruzi*-infected L6 murine muscle cells fed culture medium at 37 ºC in a 5% CO2 incubator. The results showed the severe cytotoxicity of microcystin phosphatases inhibitor [85], and of mitomycin [86], and bromodeoxyuridine [87], which is a cross linker that form DNA adducts by covalent attachment to target macromolecules. The severe cytotoxicity against the eukaryotic cells observed under the microscope consisted of loss of the cell membrane boundaries, foamy cytoplasm formation, and death.

Of interest, we noticed that the inhibitor microcystin hold blocked the formation of the 0.330 kb band, but it did not prevent the integration of the upper 1.2, 1.8 and 2.2 kb kDNA minicircle sequence bands into the macrophage genome, unlike camptothecin and bromodeoxyuridine, which did not prevent the formation of any of those bands. Nevertheless, the microcystin serine/threonine protein phosphatase inhibitor-induced cell death should undergo further study toward the development of a new drug to kill the *T. cruzi* agent of Chagas disease.

Independent assays that searched for the integration of *T. cruzi* kDNA minicircle sequences into the human macrophage genome showed an array of polymerase inhibitors of eukaryotic cell division prevented the transfer of the minicircle sequences and elimination of the 1.2, 1.8 and 2.2 kb bands (Figure 12), which was different from the situation of the

0.330 kb mitochondrial kDNA band. To approach the multidrug treatment of *T. cruzi* infections, we selected the polymerases inhibitor 4-fluorquinolone and ofloxacin [61, 62], and the azidothymidine reverse transcriptase inhibitor [51], and the lead nitro heterocycle benznidazole. The treatment of the acutely *T. cruzi*-infected BALB/c mice with benznidazole curtailed parasitemia at the 20th day of the drug administration, whereas the flagellates lasted for 40 days in the blood of the infected-untreated mice. Additionally, hemoculture, the ELISA for the specific antibody, and the *T. cruzi* nuclear DNA-PCR consistently yielded positive results for *T. cruzi*-infected mice that had received the dose of benznidazole used to treat the infection. Two out of eight mice each in the *T. cruzi*-infected-untreated and in the infected-treated groups developed identical Chagas heart disease and died with dilated cardiomegaly due to severe myocarditis. This caveat shows that the administration of benznidazole to treat *T. cruzi* infection is unsatisfactory. The information is in keeping with the observations stemmed from experimental protocols in animal models and, accordingly, with the data obtained from *T. cruzi*-infected-treated rabbits and human Chagas disease clinical trials [67-74, 88-90], although the controversy remains [91, 92]. In addition, the acutely infected mice showed parasitemia for 15 days during administration of benznidazole + azidothymidine + ofloxacin.

4.1 Insights into Human Chagas disease

Comparative pathology experiments carried out in chicken's refractory to *T. cruzi*, and in rabbits amenable to infection revealed the pathogenesis of Chagas disease stems from clones of kDNA-mutated lymphocytes, which rejected target heart cells. Initially we sought to reproduce the phenomenon in the rabbit model infection system that developed Chagas disease indistinguishable from that described in humans. The active process of genetic transfer between *T. cruzi* and rabbits was initiated with the examination of the effect of a lead benznidazole in the treatment of Chagas disease. In addition, the production of Chagas heart disease in chicken's refractory to *T. cruzi* infection, and in mice susceptible to persistent parasite infection was essential to demonstrate that lateral kDNA transfer triggers the pathogenesis of the disease.

This study aimed at the prevention of the lateral transfer of kDNA minicircle sequences into the host genome the late outcome of Chagas heart disease by administration of a multidrug cocktail of inhibitors of the main metabolic pathway checkpoints of cell growth and differentiation. First, it was found that *T. cruzi*-infected mice treated with either benznidazole and azidothymidine, or benznidazole and ofloxacin remained susceptible to the integration of the kDNA sequence into the genome. Second, the treatment of chronically *T. cruzi*-infected mouse with a cocktail of benznidazole with azidothymidine and ofloxacin produced a 2.44-fold decrease kDNA mutations in the mouse genome. Accordingly, we documented that the mice in this multidrug-treated group had reduced the severe myocarditis, comparing with those in the *T. cruzi*-infected and benznidazole-treated group.

The lateral transfer of the DNA sequence in the host cell genome is a natural consequence of *T. cruzi* infection. The intracellular invasion induces stress-related metabolic burst and cell growth that is required for minicircles to integrate into the host's genome. Therefore, growth and differentiation are among the environmental factors associated with kDNA transfer, integration, and reshuffling of the genome of the host species. The vertebrates contain repetitive short and long transposable elements (SINEs and LINEs) that persist by vertical transmission within a host, and the integration of kDNA sequences into these transposons has implications for further mobilization of foreign DNA within the genome [93]. The vertebrate genome contains a variable number of copies of retro-transposable elements [94]. Human have approximately 400 copies of active LINEs belonging to different subsets, whereas mice contain over 3,000 copies belonging to various family and type subsets [95-98]. These elements are likely progenitors of *T. cruzi* mutagenic insertions and providers of means for mobilization and reshuffling of DNA sequences around the genome, and Chagas disease over time.

4.2 Cross-Kingdom DNA Transfer, Evolution, Natural Selection, and Chagas Disease

From a historical perspective, the lateral DNA transfer phenomenon between organisms with distant evolutionary relationships is equivalent to the migration of endosymbiotic prokaryote organelles to eukaryotic cells, since approximately 2 billion years ago [99-101]. Protist mitochondrion kDNA is considered the remains of microorganisms that invaded the then emerging single-celled protozoan with a nucleus and ultimately adapted to become its own component [95]. The investigation documented a robust flow of DNA among different creatures of far-apart kingdoms. The specific detection of the *T. cruzi* kDNA minicircle fragments integrated into the genomes of vertebrate hosts is reminiscent of the microorganism assimilation of organelles such as mitochondrion and chloroplast [100], a prevailing mechanism of evolution at the molecular level. In this study, compelling evidence of lateral and vertical kDNA transfer stemmed from validation animal models' experiments. The heritable fashion of germ line cells cross-Kingdom genome growth was certainly sustained in the laboratory.

The integration of the protozoan kDNA minicircle sequence into the germline of chicken and mouse cells' LINEs and SINEs transposable elements at several chromosomes usually produced neutral mutation and positive selection [98]. However, we observed that minicircle sequences hitchhiking and kDNA sequence mobilization to coding regions, creation of new genes, and pseudogenes and silencing of genes may produce polygenic alterations and genetic mechanism of disease. The sheer number of minicircles, each with four conserved regions containing CA-rich repeat sequence motifs, may be the dominant characteristic influencing the high frequency of these serendipitous mutagenic events that influence endogenous host genes, and Chagas heart disease over time. The transposable elements that replicate within the host genome may contribute to somatic mosaicism and, thus potent regulatory polygenic modifications in the diseased state play a role in the pathogenesis of inflammatory autoimmune disease. To date, the polygenic modifications involved in the genesis of cancer [101-105] have not been ascribed to any environmental factor inducing lateral exogenous kDNA transfer. In this regard, evolution is inherently opportunistic, and Chagas heart disease could stem from the occasional onset of surreptitious alterations contributing to the activation of CD45, CD8α+ and CD8ɣð+ effector cells that express vß1 and v ß2 receptors involved in target cell rejection.

It can be suggested that the kDNA insertion mutations underpinning alterations of the effector and of the target host's cells undergo polygenic modifications, stemming from LINE-1 elements intermediate genome reshuffling, resulting in the formation of *T.* cruzi-induced autoimmune driven lesions. Although mitochondrial kDNA transfer events are neutral for the sake of species evolution, some mutations that could be deleterious hinder identification because lifelong chronically infected individuals usually retain normal health. The threatening heart disease exacerbation in approximately one third of chronically infected individuals results in a short survival of two to five years. The timely investigation of those Chagas heart disease cases revealed accumulation of lateral transfer of the kDNA mutation range from a minimum of 4 to 8 into the LINEs located on various chromosomes [106].

The refractoriness of avian to the *T. cruzi* flagellate protozoan was convenient for this study aiming at to inhibit autoimmune Chagas heart pathology because it did not require precleaning the infection. In view of the immune tolerance observed in the progeny of the Chagas disease parent, in the absence of specific antibodies, the traditional mechanism of target cell destruction by antigen-specific antibodies produced by adaptive immunity is not applicable. Therefore, the organ specificity of the autoimmune phenomenon that targets the heart is the result of germline and of somatic mutation in the genome of the effector lymphocytes and of target heart cells. Thus, each kDNA-integrated mononuclear immune cell involved in the "self" tissue destruction is essentially a mutated clone homing to the target organ where the cytotoxic lymphocyte promotes the lysis of the target cells. Disadvantageous kDNA mutation exacerbation can usually be encountered in the late phase of the disease in experimental rabbit and chicken model systems of Chagas heart disease. The mutations polygenic alterations identical to kDNA integration in a LINE-1 bringing in knockout of CLEC5A gene [50] could be a factor triggering the parasite-induced autoimmune tissue-specific rejection. Alternatively, in the absence of deleterious polygenic alteration and modification, this hypothesis could explain the long-lasting asymptomatic infection of a major parcel of *T. cruzi*-infected population, and in some patients with mutagenic kDNA fragments dispersal by active LINE-1 mobilization within the genome undergoing occasional reversal of symptoms.

4.3 Homing and Organ Specificity

Herein, knowledge stemming from molecular biology spurred histopathological insight into protist kDNA transfer into the vertebrate genome. First, the homing of the bone marrow-derived kDNA-mutated lymphocytes toward the target counterpart cells. Second, the organ specificity of the muscle and of the parasympathetic neuronal cell targets of genetically driven autoimmune rejection was informative. We postulate that selective effector-target cell signaling affinity could be a genetically acquired trait dependent upon the *T. cruzi* kDNA-integrated minicircle, showing interspersed constant and variable CSB1, CSB2 and CSB3 possible intermediates of kDNA transfer to hundreds homologous, average 8 to 25 nts share into the human genome. Additionally, we hypothesize the share repeats, folding and loop forming tri-dimensional structures, binding sites for positive and negatively charged protein electron emission signaling pathway, closed lock selection of the target for the autoimmune tissue rejection. The specificity of the target organ rejection now, called out through stoichiometry change repeats thus, DNA folding and loop tri-dimensional structures [23, 105-107], selective sites of charged proteins binding sources of cell-to-cell signaling pathway, homing, and organ selection (24, 108-109]. The signaling pathway studies of chromosome skewing and instability-generated-interactions could substantiate the organ specificity and homing, genetically driven disease mechanism ensuing rupture of immune tolerance and its eventual attenuation due to chromosome upright remodeling. We postulate that groups of kDNA minicircle sequence integration mutations, polygenic modifications, and alterations thereof, may explain lymphocyte toxicity and rejection of target host's cells in Chagas disease. Next generation scientific investigations with aid of forthcoming technologies shall unravel the deadlocks.

5 Conclusion

- The Chagas heart pathology stemmed from *T. cruzi* kDNA integrations into the genome of the mammals and of the chicken model systems, in the absence of parasitism.
- The myocarditis in the chicken refractory to the *T. cruzi* infections is identical to that of rabbits, mice, and humans.
- The inoculation of naked kDNA minicircle sequences into the fertile chicken egg did not secure the kDNA integrations.
- The kinetoplast minicircle sequences integration into the host's genome is a trans kingdom common denominator and, therefore, it can be used as a biomarker to monitor the multidrug treatment of the disease.
- The treatment of *T. cruzi*-infected mice with benznidazole, azidothymidine and ofloxacin lowered the kDNA minicircle sequences integrations and reduced the rejection of target heart cells in Chagas disease. These drugs are FDA approved for human use

Compliance with ethical standards

Acknowledgments

This work funded by the National Research Council Program for Scientific and Technological Development, CNPq/PADCT/MCT, by the Financing Study Projet-FINEP/World Bank grants, by the Brazilian Government PRONEX/FAPDF/MCT/CNPq/CAPES grant 193.000.589/2009, by the CNPq Financial Support Grant 482116/2012-9, and by the USA NIH grant R03 1164. The funders had no role in study design, data collection and interpretation or decision to submit the work for publication. All authors examined the raw data and confirmed that such representations reflect the original data and ensure that the preserved original data are retrievable. The authors acknowledge the publishers for permissions to reprint figures 6 and 9.

Disclosure of conflict of interest

The authors have declared they no competing interests.

Statement of ethical approval

The Human and the Animal Research Committees of the Faculty of Medicine of the University of Brasilia approved all the procedures with human subjects and laboratory animals research protocols 2500.167567 and 054/09, respectively. The laboratory animals received humane care; the mice under anesthesia subjected to heart puncture before sacrifice.

Authors Contributions

ARLT, designed experiments, carried out cell biology and pathology experiments, obtained tissue samples from experimental animals, and wrote the paper; CCG oversaw molecular biology study in the chicken model. AAS and AMC performed *T. cruzi* infections and parasitemia in the mouse model. RJN and LLP carried out parasitology studies in the rabbit model. FEMB oversaw the infections of fertile eggs chicken model system. AOS oversaw molecular biology study in the mouse model system.

Data information

The data set informed in this publication is retrievable at www.repositorio.unb.br. For the specific information, click the link:

S1 table: Materials, equipment's, culture cells[1], and laboratory animals [2, 3, 4]

https://repositorio.unb.br/handle/10482/45062 DADOS_S1TableNS1079054.pdf

S2 table: mapping of the sites of *Trypanosoma cruzi* kDNA integration into the rabbits' genome

https://repositorio.unb.br/bitstream/10482/43416/1/DADOS_kDNA%20integration%20rabbit%20genomesrc910173.pdf

S3 table: Mapping of the sites of integration of *Trypanosoma cruzi* kDNA minicircle sequence into the avian chromosomes.

kDNA lateral transfer to somatic cells:

https://repositorio.unb.br/bitstream/10482/43420/1/DADOS_kDNA%20integration%20chicken%20somaticsrc910173.pdf

B) kDNA Vertical transfer to chicken germ line cells:

https://repositorio.unb.br/bitstream/10482/43424/1/DADOS_kDNA%20transfer%20chicken%20germlinesrc910173.pdf

S4 table: mapping of the sites of Trypanosoma cruzi kDNA integration into the chromosome of humans.

https://repositorio.unb.br/bitstream/10482/43422/1/DADOS_Mapping%20of%20the%20sites%20human%20genomerc910173.pdf

S5 table: mapping of the sites of Trypanosoma cruzi kDNA integration into the mouse chromosomes.

https://repositorio.unb.br/bitstream/10482/43423/1/DADOS_kDNA%20integration%20mouse%20genomesrc910173.pdf

References

[1] Thomas, S., Martinez, L.L.I.T., Westernberger, S.J., Sturm N.R., A population study of the minicircles in *Trypanosoma cruzi*. Predicting guide RNAs in the absence of empirical RNA editin. *BMC Genomics*. 2007. 8,113. Doi 10.113.10.10.1186/1471-2164-8-133.

[2] Herreras-Cabello, A., Callejas-Hernandez. F., Girones, H., Fresno, M.. *Trypanosoma cruzi* genome: Organization, Multi-Gene Families, Transcription, and Biological Implications. *Genes.* 2020. 11; 1196. Doi. 10339/gene/11101196

[3] Callejas-Hernandez, F., Herreros-Cabello, A., Moral Samoral, J., Fresno, M., Girones N The complete Mitochondrial DNA of *Trypanosoma cruzi: Front. Cell Infect. Microbiol*. 2021. 11: 672 448. Doi. 103389/fcimb.2021.672448.

[4] Abras, A., Gállego, M., Muñoz, C., Juiz, N.A., Ramírez, J.C., C.I. Identification of *Trypanosoma cruzi* Discrete Typing Units (DTUs) in Latin-American migrants in Barcelona (Spain). *Parasitol. Int.* 2017. 66(2): 83-88. doi: 10.1016/j.parint.2016.12.003

[5] Strauss M, Presti MG, Ramirez J, BazanC., Kops DAV Baez, AL et al. Differential tisssue distribution of discrete type units after drug combination therapy in experimental *Trypanosoma cruzi* infection. *Parasitol.* 2021; 148(13): 1595-1601. Doi.org/1011017/5003/18202/001

[6] Souza, T.K.M., Westphalen, V.N., Westphalen, S.R., Taniguchi, H.H., Elias, R., Motoie, G. et al. Genetic diversity of *Trypanosoma cruzi* strains from chronic chagasic patients and non-human hosts in the State of São Paulo, Brazil. *Mem. Inst. Oswaldo Cruz,* Rio de Janeiro. 2022. Doi 10.1590/0074-02760220125

[7] Bern, C., Kjos, S., Yabsley, M.J., Montgomery, S.A.. *Trypanosoma cruzi* and Chagas disease in the United States. *Clin. Microbiol. Rev.* 2011. 24:655-681. Doi. 10.1128/CMR.00005-11

[8] Klein, N., Hurwitz, I., Durvasula, R. Globalization of chagas disease: A Growing Concern in Nonendemic Countries. *Epidemo. Res. Int.* 2012. doi.org/10.1155/2012/136793

[9] Pérez-Molina, J.A., Norman, F., López-Vélez, R. Chagas disease in non-endemic countries: epidemiology, clinical presentation, and treatment. *Cur. Infect. Dis. Rep*. 2012. 14:263-74. doi: 10.1007/s11908-012-0259-3.

[10] Lidani, K.C.F, Andrade, F.A., Damasceno, F.S., Beltrame, M.B., Iaram J., Messias-Reason, I.J., et al. Chagas Disease: From Discovery to a Worldwide Health Problem. *Front. Pub. Health*. 2019. doi.org/10.3389/fpubh.2019.00166

[11] Teixeira, A.R.L., Nascimento, R., Sturm, N.R. Evolution and Pathology in Chagas disease. *Mem. Inst. Oswaldo Cruz*. 2006. 101:463-491.

[12] Prata, A. Clinical and epidemiological aspects of Chagas disease. *The Lancet*. 2001. 1: 92-100. Doi.org/10.1016/S1473-3099(01)00065-2

[13] Almeida, A.B., Araújo, P. F., Bernal., F.E.M., Rosac A.C.,Valente, S.A., Teixeira, A.R.L.. Sexual Transmission of American Trypanosomes from Males and Females to Naive Mates. *J. Visual. Exp*. 2019.143: e57985. Doi: 10.3791/57985

[14] Gomes, C. Santos, J.E., Silveira-Lacerda, E., Baliza, M., Teixeira, A.R.L.. Blood transfusion and diagnostic accuracy of chagas disease. *J. Bacteriol. Mycol*. 2019b. 7:112-114. Doi.10.15406/jbmoa.2019.07.00255

[15] Coura, J.R., Dias, J.C.P. Epidemiology, control, and surveillance of Chagas disease: 100 years after its discovery. *Mem. Int. Oswaldo Cruz*. 2009. 104 (supl 1). Doi.org/10.1590/S0074-02762009000900006

[16] Teixeira A.R.L., Vinaud, M., Castro, A.M. (2009). In: Emerging Chagas Disease. Chapter: The Pathology of Chagas disease, pp. 104-109. Chapter: *Trypanosoma cruzi* infection in human hosts. Pp. 110-121. Bentham Books. Doi 10.2174/9781 6080 5041131090101

[17] Dias, J.C.P. Human Chagas Disease and Migration in the Context of Globalization: Some Particular Aspects. *J. Trop. Med*. 2013. Doi.org 10.1093/clinids/6.2.223

[18] Molina, I., Perin, L., Aviles, A.S., Vieira, P.M.A., Fonseca, K.S., Cunha, L.M., et al. The effect of benznidazole dose among the efficacy outcome in the murine animal model. A quantitative integration of the literature. *Acta. Trop*. 2019. 105218. doi: 10.1016/j.actatropica.2019.105218

[19] Cunha, E.L.A., Torchelsen, F.K.V.S., Cunha L.M., Oliveira, MT,. Silva, K., Fonseca, P. et al. Benznidazole, itraconazole and their combination in the treatment of acute experimental Chagas disease in dogs. *Exp. Parasitol*. 2019. 204:107711. Doi: 10.1016/j.exppara. 2019.05.005

[20] de Jesus, S.M., Pinto, L., Moreira, F.L., Nardotto, G.H.B., Cristofoletti, R., Perin, L. Pharmacokinetics of Benznidazole in Experimental Chronic Chagas Disease Using the Swiss Mouse-Berenice-78 *Trypanosoma cruzi* Strain Model. *Antimicrob. Agents. Chemother*. 2021. 65: e01383-20. Doi: 10.1128/AAC.01383-20

[21] Docampo, R.. Sensitivity of parasites to free radical damage by antiparasite drugs. *Chem. Biol. Interact*. 1990. 73:1-27. doi: 10.1016/0009-2797(90)90106-w

[22] McKerrow, J.H. Update on drug development targeting parasite cysteine proteases. *PLoS Negl. Trop. Dis.* 2018. 12: e0005850. Doi.org/10.1371/jounal.pntd.0005850

[23] Teixeira, A.R., Gomes, C., Nitz, N., Sousa, A.O., Alves, R.M., Guimaro, M.C., et al.. *Trypanosoma cruzi* in the Chicken model: Chagas-like heart disease in the absence of parasitism. *PLoS Negl. Trop. Dis*. 2011a. 5: e1000. Doi: 10.371/jornal pntd.0001.1000

[24] Prado, C.M., Celes, M.R.N. Malvestio, L.M., Campos, E.C., Silva, J.S., Jelicks, L.A., et al. Early dystrophin disruption in the pathogenesis of experimental chronic Chagas cardiomyopathy. *Microbes Infect*. 2012. 14-59-68. Doi.org./10.1016/j.micinf.2012.08.10

[25] Lewis, M.D., and Kelly, J.M. Putting Infection Dynamics at the Heart of Chagas Disease. *Trends Parasitol*. 2016. 32:899–911. doi: 10.1016/j.pt.2016.08.009

[26] Bonney, K.M., Luthringer, D.J., Kim, S.A., Garg, N.J., Engman, D.M. Pathology and Pathogenesis of Chagas Heart Disease. *Annu. Rev. Pathol*. 2019. 14:421-427. Doi: 10.1146/annurev-pathol-020117-043711

[27] Wesley, M., Moraes, W.M., Rosa, A.C., Carvalho, J.L., Shiroma, T., Vital, T., et al. Correlation of Parasite Burden, kDNA Integration, Autoreactive Antibodies, and Cytokine Pattern in the Pathophysiology of Chagas Disease. *Front. Microbiol*. 2019. 10: 1856. doi.org/10.3389/fmicb.2019.01856

[28] Teixeira, P.C., Ducret, A., Langen, H., Nogoceke, E., Santos, R.H.P, Nunes, J.P.S. Impairment of multiple mitochondrial energy metabolism pathways in the heart Chagas disease cardiomyopathy patients. *Front. Immunol.* 2021. *Doi.org*. /103389/fimmu.2021.755782

[29] Brochet, P., Ianni, B.M., Langier, L., Frade, A.F., Teixeira, P.C. Epigenetic regulation of transcription factor binding motifs promotes Th1 response in Chagas disease cardiomyopathy. *Front Immunol*. 2022; 13:958200. Doi: 103389/fimmu.2021.755782

[30] Teixeira, A.R.L., Argañaraz, E.R., Freitas Jr, L.H., Lacava, Z.G., Santana, J.M., Luna, H. Integration of Trypanosoma cruzi kDNA minicircles into the host cell genome by infection. *Mutat. Res*. 1994b. 305:197-209. doi: 10.1016/0027-5107(94)90240-2

[31] Teixeira, A.R.L, Teixeira, M.L., Santos Buch, C.A. The immunology of experimental Chagas' disease. IV. Production of lesions in rabbits similar to those of chronic Chagas' disease in man. 1975; 80(1): 163–180. *Am. J. Path.* 1975. PMID: 808136

[32] Ramirez, L.E. and Brenner, Z. Evaluation of the rabbit as a model for Chagas disease: I. Parasitological studies. *Mem. Inst. Oswaldo Cruz*. 1987. 82:4. doi: 10.1590/s0074-02761987000400010

[33] Teixeira, A.R., Córdoba J.C., Souto Maior, I., Solórzano, E.. Chagas disease: Lymphoma growth in rabbits treated with Benznidazole. *Am. J. Trop. Med. Hyg*. 1990a. 43:146-158. doi.org/10.4269/ajtmh.1990.43.146

[34] Silva, A.M., Ramirez, L.E., Vargas, M., Chapadeiro, E., Brener, Z.. Evaluation of the rabbit as a model for Chagas disease - II: histopathologic studies of the heart, digestive tract, and skeletal muscle. *Mem. Inst. Oswaldo Cruz*. 1996. 91. doi.org/10.1590/50074-02761996000200015

[35] Santos-Buch CA, Teixeira ARL. The immunology of expeirmental Chagas disease. III. Rejection of allogeneic heart cells in vitro. 1974. *J. Exp. Med*. 140: 38-39.

[36] Kierszenbaum, F. Antibody-Independent, Natural Resistance of Birds to Trypanosoma cruzi Infection. *J. Parasitol*. 1981. 67:656-660. PMID: 6795329

[37] Canning, P.P., Kwangjin, P., Gonçalves, J., Conor, C.L., Howard, J., Sharpe, T.D. CDKL Family Kinases Have Evolved Distinct Structural Features and Ciliary Function. *Cell Rep*; 2018. 22(4): 885-894. Doi.org/10.1016/j.celrep.2017.12.083.

[38] Wozniak, J.M., Silva, T.A., Thomas D., Siqueira-Neto J.L., McKerrow, J.H., Gonzalez, D.J., et al.. Molecular dissection of Chagas induced cardiomyopathy reveals central disease associated and druggable signaling pathways. *PLoS Negl. Trop. Dis*. 2020.14: e0007980. doi: 10.1371/journal.pntd.0007980

[39] Zhang, W.L., and Tu, H. MAPK signal pathways in the regulation of cell proliferation in mammalian cells. *Cell Res*. 2002. 12(1):9-18. DOI:10.1038/sj.cr.7290105

[40] Arthur, J.S., and Ley, S. Mitogen-activated protein kinases in innate immunity. Mitogen-activated protein kinases in innate immunity. *Nat. Rev. Immunol*. 2013. 13:679–962. doi.org/10.1038/nri3495

[41] Burotto, M., Chiou, V.L., Jung-Min, L., Kohn, E. C. The MAPK pathway across different malignancies: a new perspective. *Cancer*. 2014. 120(22):3446-56. Doi: 10.102/cncr.28864

[42] Guo, Y-J., Pan, W-W., Liu, S-B., Shen, Z-F., Xu, Y., Hu, L-L. ERK/MAPK signaling pathway and tumorigenesis (Review). *Exp. Ther. Med.* 2020. doi.org/10.3892/etm.2020.8454

[43] Buckner, F.S., Wilson, A.J., Van Voorhis, W.C. Detection of live *Trypanosoma cruzi* in tissues of infected mice by using histochemical stain of β-galactosidase. *Infect. Immun.* 1999. 67:403-409. Doi: 10.128/IAI.67.1.403-409.1999.

[44] Araújo, P.F., Almeida, A.B., Pimentel, C.F., Silva, A.R., Sousa, A.O, Valente, A.S., et al. Sexual transmission of American trypanosomiasis in humans: a new potential pandemic route for Chagas parasites. *Mem. Inst. Oswaldo. Cruz*. 2017. 112:437-446. Doi: 10.1590/00760 160538

[45] Guimaro, M.C., Alves, R.M., Rose, E., Sousa, A.O., Rosa, A.C., Hecht, M. et al. Inhibition of autoimmune Chagas-like heart disease by bone marrow transplantation. *PLoS Negl.Trop. Dis*. 2014. 8: e3384. doi: 10.1371/journal.pntd.0003384

[46] Sturm, N.R., Degrave, W., Morel. C., Simpson, L. Sensitive detection and schizodeme classification of *Trypanosoma cruzi* cells by amplification of kinetoplast minicircle DNA sequences: use in diagnosis of Chagas disease. *Mol. Biochem. Parasitol.* 1989. 33:205-214. Doi: 10.1016/0166-6851(89)90082-0

[47] Moser, D.R., Kirchhoff, L.V, Donelson, J.E. Detection of *Trypanosoma cruzi by* DNA amplification using the polymerase chain reaction. *J. Clin. Microbiol*. 1989. 27: 1477-1482. PMID: 8408566

[48] Murthy, V.K., Dibbem, K.M., Campbell, D.A. PCR amplification of mini-exon genes differentiates *Trypanosoma cruzi* from *Trypanosoma rangeli*. *Mol. Cell Probes*. 1992. 6:237-243. doi: 10.1016/0890-8508(92)90022-p.

[49] Requena, J.M., Jimenez-Ruiz, A., Soto, R.M., Lopez, M.C., Alonso, C. Characterization of a highly repeated interspersed DNA sequence of *Trypanosoma cruzi:* its potential use in the diagnosis and strain classification. *Mol. Biochem. Parasitol.* 1992. 51: 271-280. PMID: 1574085

[50] Teixeira, A.R., Hecht, M.M., Guimaro, M.C., Sousa, A.O., Nitz N. Pathogenesis of Chagas disease: parasite persistence and autoimmunity. *Clin. Microbiol. Rev*. 2011b. 24: 592–630. Doi: 10.1128/CMR.00063-10

[51] Árquez. M.A., Martín-Alonso, S., Gorelick, R.J., Scott, W.A., Acosta-Hoyos, A.J., Menéndez-Arias, L. Nucleocapsid Protein Precursors NCp9 and NCp15 Suppress ATP-Mediated Rescue of AZT-Terminated Primers by HIV-1 Reverse Transcriptase. *Antimicrob. Agents Chemother*. 2020. 64: e00958-20. Doi: 10.1128/AAC.00958-20

[52] Condezo, G.N., San Martin, C. Bromodeoxyuridine Labeling to Determine Viral DNA Localization in Fluorescence and Electron Microscopy. The Case of Adenovirus. *Viruses*. 2021. 13(9):1863. Doi. 10.3390/v13091/v13091863

[53] Forkosh.E., Kenig. A., Ilan. Y. Introducing variability in targeting the microtubules: Review of current mechanisms and future directions in colchicine therapy. *Pharmacology Research & Perspective*. 2020 doi.org/10.1002/prp2.616

[54] Tuli, H.S., Muobarak, M.J., Thakral, F., Sak, K., Kumar, M., Kumar, A., et al. Molecular Mechanisms of Action of Genistein in Cancer. *Front. Pharmccol*. 2019. Doi. 10.3389/fphar.2019.01336.

[55] Adamovsky, O., Buerger, A.N., Wormington, A.M., Ector, N., Griffitt, R.J., Bisesi Jr., J.H., et al. The gut microbiome and aquatic toxicology: an emerging concept for environmental health. *Environ. Toxicol. Chem*. 2018. 37:2758–2775. Doi.org/10.1002/etc.4249

[56] Ramos, D.F., Matthiensen, A., Colvara, W., de Votto, A.P..S, Trindade, G.S., da Silva, P.E.A. et al. Antimycobacterial and cytotoxicity activity of microcystins. *J. Venom Anim. Toxins Trop. Dis*. 2015. Doi.org/10.1186/s40409-015-0009-8

[57] Heller, B.M., David, J., Marmion, D.J., ., Thompson, C.A, Carrie, A.C., et al. Mitomycin-C treatment during differentiation of induced pluripotent stem cell-derived dopamine neurons reduces proliferation without compromising survival or function in vivo. *Stem Cells Transl Med*. 2021. 10: 278–290. Doi: 10.1002/sctm.20-0014

[58] Bedi, D., Henderson, H.J., Manne, U., Temesgen, S. Camptothecin Induces PD-L1 and Immunomodulatory Cytokines in Colon Cancer Cells. *Medicine*. 2019. Doi: 10.3390/medicines6020051

[59] Wang L, Gundelach. J.H., Bram, R.J. Cycloheximide promotes paraptosis induced by inhibition of cyclophilins in glioblastoma multiforme. *Cell Death Dis.* 2020. 18: e2807. Doi:101038/cddis.2017.217

[60] Ferreira de Oliveira, J.M.P., Pacheco, A.R., Coutinho, L., Oliveira, H., Pinho, S., Almeida, L., et al. Combination of etoposide and fisetin results in anti-cancer efficiency against osteosarcoma cell models. *Arch. Toxicol*. 2018. 92:1205-1214.Doi: 10.1007/s00204-017-2146-z

[61] El-Rayes, B.F., Grignon, R., Slam, N., Aranha, O., Sarkar, F.H. Ciprofloxacin inhibits cell growth and synergesis the effect of etoposide in hormone resistant prostate cancer. *Int. J. Oncol*. 2002. 21:207-11. PMID: 12063570

[62] Adasme, M.A., Bolz, S.N., Adelmann, L., Salentin, S.V., Haupt, J., Moreno-Rodríguez, A., et al. Repositioned Drugs for Chagas Disease Unveiled via Structure-Based Drug Repositioning. *Int. J. Mol. Sci*. 2020. 21:8809. Doi.10.3390/ijms21228809

[63] Tarazi, H., Saleh, E., El-Awardi, R. In silico screening of DNA-dependent protein kinase (DNA-PK) inhibitors: Combined homology modeling, docking, molecular dynamic study followed by biologic investigation. *Biomedicine & Pharmacology*, 2016. 83: 693-703. Doi.org/101016/j.biopha.2016.07.044.

[64] Chakrabarty, S., Nag. D., Ganguli, A., Das, A., Dastidar, G.D., Chakrabarty, G. The aflavin and epigallocaechin-3-gallate sinergistically induce apoptosis through inhibition of PI3K/Akt signaling upon depolymerizing microtubules in HeLa cells. *J. Cel. Biochem*. 2019. 120:5987-6003. Doi. 0.1002/jcb.27886

[65] Gonçalves, A.P., Videira, A., Maximo, V., Soares, P. Synergistic growth inhibition of cancer cells harboring the RET/pTCI oncogene by staurosporine, and rotenone involves enhanced cell death. *J. Biosci*. 2011. 36:639-48. Doi: 10.10007/s12038-011-9100-7.

[66] Hecht, M.M., Nitz, N., Araújo, F.P., Sousa, A.O., Rosa, A.C., Gomes, D.A. et al. Inheritance of DNA transferred from American trypanosomes to human hosts. *PLoS ONE.* 2010. 5: e9181. doi.org/10.1371/journal.pone.0009181

[67] Teixeira, A.R., Nitz, N., Bernal, F.M., Hecht, M.M. Parasite induced genetically driven autoimmune Chagas heart disease in the chicken model. *J. Vis. Exp.* 2012. 29:3716. doi: 10.3791/3716

[68] Lauria-Pires, L., Braga, M.S., Vexenat, A.C., Nitz, N., Simões-Barbosa, A., Tinoco, D.L. et al. Progressive chronic Chagas heart disease ten years after treatment with nitroderivatives. *Am. J. Trop. Med. Hyg*. 2000. 63(3-4):111-8. doi: 10.4269/ajtmh.2000.63.111

[69] Morillo, C.A., Marin-Neto, J.A., Avezum, A., Sosa-Estani, S., Rassi-Jr., A. Randomized Trial of Benznidazole for Chronic Chagas' Cardiomyopathy. *N. Engl. J. Med*. 2015. 373:1295-1306. DOI: 10.1056/NEJMoa1507574

[70] Viotti R, Vigliano C, Lococo B, Bertochi G, Vigliano C. et al. Long-term cardiac outcomes of treating chronic Chagas disease with benznidazole versus no treatment: a nonrandomized trial. *Ann Intern Med.* 2006. May 16; 144:724-34. doi: 10.7326/0003-4819-144-10-200605160-00006

[71] Schmidt, A., Romano, M.D., Marin-Neto, J.A., Rao-Melacini, P., Rassi Jr. A., Mattos, A. et al. Effects of Trypanocidal Treatment on Echocardiographic Parameters in Chagas Cardiomyopathy and Prognostic Value of Wall Motion Score Index: *J. Am. Soc. Echocardiology*. 2019. 32: 286-295. doi: 10.1016/j.echo.2018.09.006

[72] Crespillo-Andújar C, Comeche B, Hamer DH, Arevalo-Rodriguez I, Alvarez-Díaz, N et al. Use of benznidazole to treat chronic Chagas disease: An updated systematic review with a meta-analysis. 2022, May 16. https://doi.org/10.1371/journal.pntd.0010386

[73] Teixeira ARL, Calixto MA, Teixeira ML.. Chagas' disease: carcinogenic activity of the antitrypanosomal nitroarenes in mice. *Mut. Res.* 1994a. 305: 189-196. Doi: 10.1016/0027-5107(94)90239-9

[74] Teixeira, A.R.L., Cunha Neto, E., Rizo, L.V., Silva, R. Trypanocidal nitroarene treatment of experimental *Trypanosoma cruzi* infection does not prevent progression of chronic phase heart lesions in rabbits. *J. Infect. Dis.* 1990b.162:1420. Doi.org/101093/infdis/162.6.1420.

[75] Huss, D.J., Saias, Sl, Hamamah, S., Singh, J.M., Wang, J., Dave, M., et al. Matrix During Early Migration. *Front. Cell. Dev. Biol*. 2019. Doi10.3389/fcell.2019.00035/

[76] Simões-Barbosa A, Argañaraz ER, Barros AM, Rosa AC, Alves NP, Louvandini, P. et al. Hitchhiking Trypanosoma cruzi minicircle DNA affects gene expression in human host cells via LINE-1 retrotransposon. *Mem. Inst. Oswaldo Cruz*. 2006. Doi. 10.3410/f.1060778.512704

[77] Cronemberger-Andrade, A.,Xander, P., Soares, R.P., Pessoa, N.L., Campos, M.A., Cameron, C., et al. *Trypanosoma cruzi*-Infected Human Macrophages Shed Proinflammatory Extracellular Vesicles That Enhance Host-Cell Invasion via Toll-Like Receptor 2. *Front. Cell. Infect. Microbiol*. 2020. doi.org/10.3389/fcimb.2020.00099

[78] Teixeira ARL, Calixto MA, Teixeira ML.. Chagas' disease: carcinogenic activity of the antitrypanosomal nitroarenes in mice. Mut Res. 1994; 305: 189-196. Doi: 10.1016/0027-5107(94)90239-9

[79] Leon, J.S., Daniels, M.D., Toriello, K.M., Wang, K., Engmam, D.M. A cardiac myosin-specific autoimmune response is induced by immunization with *Trypanosoma cruzi* proteins. *Infect. Immun*. 2004. 72: 3410-3417. doi: 10.1128/IAI.72.6.3410-3417.2004

[80] Jiménez,P., Jesús J., Poveda, C., Ramírez, J.D. A systematic review of the *Trypanosoma cruzi* genetic heterogeneity, host immune response and genetic factors as plausible drivers of chronic chagasic cardiomyopathy. *Parasitol.* 2019. 146(3): 269-283. doi: 10.1017/S0031182018001506

[81] Cunha-Neto, E., Bilate, A.M., Hyland, K.V., Fonseca, S.G., Kalil, J., Engman. D.M. Induction of cardiac autoimmunity in Chagas heart disease: a case for molecular mimicry. *Autoimmunity*. 2006. 39: 41-45. DOI: 10.1080/08916930500485002

[82] Bonney, K.M., Taylor, J.M., Daniels, M.D., Epting, C.L., Engman, D.M. Heat-killed *Trypanosoma cruzi* induces acute cardiac damage and polyantigenic autoimmunity. *PLoS ONE* 2011. 6: e14571. Doi: 10.1371/journal.pone.0014571

[83] Abel, I.C., Rizzo, L.V., Ianni, B., Albuquerque, F., Bacal, F. et al. Chronic Chagas disease cardiomyopathy patients display an increased IFN-gamma response to *Trypanosoma cruzi* infection. *J. Autoimmun.* 2001. 17: 99-107. doi: 10.1006/jaut.2001.0523

[84] Vicco MH, Ferini C, Lococo B, Bertochi C, Petti M, et al. Long-term cardiac outcomes of treating chronic Chagas disease with benznidazole versus no treatment: a nonrandomized trial. *Ann Intern Med.* 2006. 144 (10): 724-34. Doi: 107326/0003-4819-144-10-200605-00006

[85] Chatelain, E., Scandale, I. Animal models of Chagas disease and their translational value to drug development. *Exp. Op. Drug. Discov*. 2020. 5: 1381-1402. Doi: 10.1080/17460441.2020.1806233

[86] Árquez. M.A., Martín-Alonso, S., Gorelick, R.J., Scott, W.A., Acosta-Hoyos, A.J., Menéndez-Arias, L. Nucleocapsid Protein Precursors NCp9 and NCp15 Suppress ATP-Mediated Rescue of AZT-Terminated Primers by HIV-1 Reverse Transcriptase. *Antimicrob. Agents Chemother*. 2020. 64: e00958-20. Doi: 10.1128/AAC.00958-20

[87] Adasme, M.A., Bolz, S.N., Adelmann, L., Salentin, S.V., Haupt, J., Moreno-Rodríguez, A., et al. Repositioned Drugs for Chagas Disease Unveiled via Structure-Based Drug Repositioning. *Int. J. Mol. Sci*. 2020. 21:8809. Doi.10.3390/ijms21228809

[88] Condezo, G.N., San Martin, C.. Bromodeoxyuridine Labeling to Determine Viral DNA Localization in Fluorescence and Electron Microscopy. The Case of Adenovirus. *Viruses*. 2021 13(9):1863. Doi. 10.3390/v13091/v13091863

[89] Braga, M.S., Lauria-Pires, L., Argañaraz, E.R., Nascimento, R.J., Teixeira, A.R.L. Persistent infections in chronic Chagas' disease patients treated with anti-*Trypanosoma cruzi* nitroderivatives. *Rev. Inst. Med. Trop. São Paulo*. 2000. 42:157-61. Doi: 10.1590/s0036-46652000000300009

[90] Moscatelli, G.T., Moroni, S., Bournissen F.G, González, N., Ballering, G., Schijman A. et al. Longitudinal follow up of serologic response in children treated for Chagas disease. *PLoS Negl. Trop. Dis*. 2019. Doi/org 10.371/journal.pntd. 0007668

[91] Caldas, I.S., Santos, E.G. Novaes, R.D. An evaluation of benznidazole as a Chagas disease therapeutic, *Expert Opinion on Pharmacotherapy.* 2019. 20:15, 1797-1807, DOI: 10.1080/14656566.2019.1650915

[92] Morais, T.R., Conserva, G.A.A, Varela, M.T. Improving the drug-likeness of inspiring natural products - evaluation of the antiparasitic activity against *Trypanosoma cruzi* through semi-synthetic and simplified analogues of licarin A. *Sci. Rep*. 2020. Doi.org/10.1038/s41598-020-62352-w

[93] Torrico, F., Gascon, J., Barreira, F., Blum, B., Almeida, I.C., Alonso-Veja, C., et al. Benznidazole monotherapy and combination with fosravuconazole for treatment of Chagas disease (Bendita): a phase 2 double-blind, randomised trial. *The Lancet Infect. Dis.* 2021. 21: 129-140 doi. 10.1016/S1473-3099(20)30844-6.

[94] Brouha, B., Schustak, J., Badge, R.M., Lutz-Prigge, S., Farley, A.H., Moran, J.V., et al. Hot L1s account for the bulk of retrotranposition in the human population. *Proc. Nat. Acd. Sci.* USA. 2003. 100:5280-5. Doi: 10.1073/pnas.0831042100

[95] Hajduk, S.C., Wang, L., Zhou, L., Zhao, Y. Cassavant, N.C., Huang, S. LINE-1 (L-1) lineages in the mouse. *Mol. Biol. Evol*. 2000. 17: 616-628. doi.org/10.1093/oxfordjournals.molbev.a026340

[96] Buschman, F. (2002). Lateral DNA Transfer. Mechanisms and Consequences. Chapter 2, in: DNA and Lateral Transfer pp 15-260. Cold Spring Harbor Laboratory Press, Cold Spring Harbor, New York

[97] DeBarry, J.D., Ganko, E.W., McCarthy, E.M., McDonald, J.F. The contribution of LTR retrotransposon sequences to gene evolution in Mus musculus. *Mol. Biol. Evol*. 2006. 23:479-481. Doi: 10.1093/molbev/msj076

[98] Sciamanna, I., Vitullo, P., Curatolo, A., Spadafora, C. Retrotransposons, reverse transcriptase, and the genesis of new genetic information. *Gene.* 2009. 448:180-1866. Doi: 10, 1016/j.gene.2009.07.011

[99] Hancks, D.C., Kazazian Jr., H. Roles for retrotransposon insertions in human disease. *Mobile DNA*. 2016. 7:9.

[100] Klein, J., Takahata, N. (2002). Where do we come from? The molecular evidence for human descent. Chapter 10, in: The narrow road to the deep North, pp 249-314. Springer-Verlag Berlin, Heidelberg, New York. Doi: 10.1007/978-3-662-04847-4

[101] Margulis, L. and Sagan, D. (2002). Acquiring genomes. A theory of the origin of species. Chapter 2: pp 25-50. Basic Books, New York. University of Massachusetts, Amherst Massachusetts

[102] Saleh, A., Macia, A., Muotri, A.R. Transposable Elements, Inflammation, and Neurological Disease *Front. Neurol.* 2019. doi.org/10.3389/fneur.2019.00894

[103] Cervantes-Ayalc, A., Garrido, R.E., Velazquez, M.A. Long Interspersed Nuclear Elements 1 (LINE1): The chimeric transcript L1-MET and its involvement in cancer. *Cancer Genetics*. 2019. Doi: 10.1016/j.cancergen.2019.11.004

[104] Ponomaryova, A.A., Rykova, E.Y., Gervas, P.A., Cherdyntseva, N.V., Mamedov, I.Z., Azhikina, T.L. Aberrant Methylation of LINE-1 Transposable Elements: A Search for Cancer Biomarkers. *Cells Review*. 2020 doi: 10.3390/cells9092017

[105] Grundy, E.E., Diab, N., Chiappinelli, K.B. Transposable element regulation and expression in cancer *FEBS J.* 2021. doi.org/10.1111/febs 15722

[106] Shapiro, J.A. How Chaotic Is Genome Chaos? *Cancers.* 2021. Doi. org.10,3390/cancers 13061358.

[107] Lieberman-Aiden, E., van Berkum, N.L., Williams, L., Imakaev, M., Ragoczy T., Telling, A., et al. Comprehensive mapping of long-range interactions reveals folding principles of the human genome. *Science.* 2009. 326:289-93. Doi: 10.1126/science.1181369

[108] Mantoni, F., Torelli, S., Ferline, A. Dystrophin and mutations; one gene several proteins, multiple phenotypes. *Lancet Neurol*. 2010. 2: 731-740. Doi. org. /10.1961/S1474-4422 (03) 00585-4

[109] Mukherjee, A., Roy, S., Saha, B., Mukherjee, D. Spatio-Temporal Regulation of PKC Isoforms Imparts Signaling Specificity. *Front. Immunol*. 2016. doi.org/10.3389/fimmu.2016.00045